Ultraviolet laser photodesorption of NO from condensed films: Translational and internal energy distributions

W. C. Natzle,[a] D. Padowitz, and S. J. Sibener[b]
Department of Chemistry and The James Franck Institute, The University of Chicago, Chicago, Illinois 60637

(Received 2 December 1987; accepted 10 March 1988)

In this paper we report that ultraviolet laser induced desorption from the surface of a thin nitric oxide film proceeds via two mechanisms which are present simultaneously. One mechanism is attributed to laser induced thermal desorption while the other is due to a nonthermal, single photon process. A film of 1–2000 ML (layers) of NO condensed on a Ag(111) substrate under UHV conditions at 25–50 K was irradiated by 5 ns pulses of 220–270 nm laser light (4.6–5.5 eV) with 0.5–5 mJ/cm^2 (0.1–1 MW/cm^2) power density at the surface. Translational energies of desorbed molecules were measured from time-of-flight (TOF) spectra taken with a mass spectrometer, while the internal energy distribution of molecules desorbed in the nonthermal channel was determined by a (1 + 1) resonance enhanced multiphoton ionization (REMPI) probe. NO monomer in the $^2\Pi_{3/2,1/2}$ electronic ground states was the only significant product. There were two distinct characteristic TOF components, which we associate with different desorption mechanisms. Each component had a different velocity and angular distribution, and their relative yields varied with laser pulse energy and NO layer thickness. Under conditions where both mechanisms gave comparable desorption yields, we obtained TOF distributions which were bimodal. A "slow" peak with an average translational energy up to 0.06 eV was Maxwellian with temperatures between 160 and 280 K and a broad angular distribution. Yield in this peak increased strongly with layer thickness and exponentially with laser pulse energy. A "fast" TOF peak with average energy of 0.22 eV was non-Maxwellian, with an angular distribution peaked toward normal, and yield increasing linearly with laser pulse energy. REMPI of the fast peak showed a vibrational population ratio $v = 3$:$v = 2$ of 0.85. A Boltzmann plot of the rotational population distribution of $v = 2$ molecules, if fit with a single line, gave a temperature of 2500 K. We use these angular, velocity, rotational, and vibrational distributions to suggest mechanisms for the nonthermal desorption. We also discuss factors determining the relative extent of thermal and photochemical effects, which control the morphology of ablated surfaces.

I. INTRODUCTION

Laser–surface interactions are increasingly important in science and technology. In industry, lasers cut, weld, and anneal materials—all thermal processes. In microelectronics and medicine, ultraviolet lasers can precisely etch or ablate polymer films or biological tissues with little heat damage. This remarkable new technique appears to involve both thermal and nonthermal photochemical mechanisms.[1] What determines the extent of thermal and nonthermal effects, and what are the photochemical processes induced in condensed matter by ultraviolet radiation? These questions may be impossible to answer for complex technological materials. We have therefore studied a simple model system in which laser and film characteristics can be well controlled, and the molecules removed from the film can be examined in detail. In these experiments we have used UV excitation of a molecular film condensed on a metal substrate, followed by translational and internal energy measurements of desorbed molecules, to study desorption mechanisms and energy flow pathways during UV photodesorption.

In surface science, laser surface interactions serve both as probes of surface structure and dynamics, and in their own right as important new phenomena. Many laser induced surface and adsorbate–surface phenomena have been recognized.[2] Lasers can rapidly heat substrates, or directly excite vibrations or electronic states in surfaces or adsorbates. We first review a few results relevant to our work from laser thermal desorption, infrared photodesorption, and ultraviolet photodissociation on surfaces.

A. Laser heating of substrates

Laser induced thermal desorption (LITD) with nano- or picosecond pulse lengths can produce heating rates of 10^{12} K/s or higher, yielding high densities of desorbing molecules above the surface. If LITD is studied for clues to the dynamics of the desorption process, care must be taken to eliminate collisional perturbations of desorbing molecules. During early work in this area, non-Maxwellian TOF distributions were seen in D_2 desorbed from W by heating the substrate with 1060 nm IR light, but the distributions had been distorted by collisions.[3] Wedler *et al.*[4] heated a CO covered Fe(110) surface and measured Maxwellian TOFs which were lower than the surface temperature for surfaces hotter

[a] Current address: IBM East Fishkill, Z/340, Rte. 52, Hopewell Junction, New York 12533.
[b] Alfred P. Sloan Fellow, 1984–1987.

 0021-9606/88/127975-20$02.10

than 600 K. Burgess and various co-workers have studied desorption of CO from Cu substrates heated with UV lasers. They measured Maxwellian TOF distributions below the predicted surface temperature, with no evidence of collisions, although desorbed fluxes were high.[5] More recently, they have observed non-Maxwellian TOF distributions with two components, and obtained laser fluorescence state resolved rotational and TOF data, which should provide a detailed picture of the energy distribution in the desorbing molecules.[6]

B. Laser excitation of adsorbates and covalently bonded surfaces

If a molecule on or near a surface is directly excited by photons with enough energy, it might desorb before all of the excitation dissipates. Of course thermal desorption may follow, but we are most interested in cases where equilibration of energy is incomplete at the time of desorption. We will call this photochemical, or simply nonthermal, desorption. A major question in laser induced desorption is the relative role of thermal vs nonthermal mechanisms. Because these mechanisms imply different energy disposal and often different desorption dynamics, they may be distinguished, and insights into the desorption process obtained, by measuring the translational and internal energy distributions of the desorbed species.

The nonstatistical energy distributions of photochemically desorbed molecules may reveal their history subsequent to excitation. Excited molecules at a surface are few and short lived, requiring fast, sensitive probes to follow their dynamics.[7-9] Desorption can be prompt enough to compete with bulk or surface relaxation processes. This competition will be reflected in the energy distributions of the desorbed species, which can then be determined with sensitive gas phase techniques. If the quantum yield and total energy of desorbed products is known, conservation of energy gives the amount left behind in the surface, and we may be able to determine branching ratios for relaxation and desorption mechanlsms. Thus the desorbed molecules can serve as a window into energy flow at a surface.

1. Infrared excitation

Infrared lasers can deposit energy directly into adsorbate–surface vibrations or internal vibrational modes of adsorbates. Desorption following resonant infrared excitation has been studied by several groups.[10,11] Chuang and coworkers have looked for "quantum effect" desorption—absorption of IR photons by a surface vibrational mode, followed by desorption of the excited species without thermal equilibration of the absorbed energy in the surrounding adsorbate layer or the substrate lattice. As the laser wavelength is tuned through an absorption band, resonant desorption is seen, but not desorption that is selective between coadsorbed isotopically substituted species. In IR experiments, the energy of a single photon is usually less than required to break the surface bond, and several processes—direct substrate heating, indirect or resonant heating of the substrate through adsorbate absorption of laser light, and resonant heating of multilayer adsorbate films—contribute to thermal desorption that can obscure any multiphoton quantum desorption. To understand these processes, theoretical calculations of vibrational energy transfer between adsorbates, electronic damping of vibrations by the surface, and desorption have been performed.[11,12]

2. Ultraviolet excitation

Electronic excitation of adsorbates by ultraviolet light opens new channels for energy transfer. A single UV photon provides energy comparable to a chemical bond, and an excited molecule is more likely to dissociate, react photochemically or desorb before the excitation is damped or thermalized. Elucidation of these multiple pathways is just beginning: there is phenomenology but only a few theoretical treatments.[12,13] Experiments in thin film processing and surface photochemistry have looked at film morphology after irradiation or demonstrated photoinduced reactions on the surfaces of semiconductors,[14-18] rough silver,[19] inorganic substrates, thin physisorbed films, and organic polymers.[2,20-22] Again, measurements of energy distributions may be useful in distinguishing thermal from photochemical processes. Only a few researchers have measured energy disposal in photochemical reaction products or in desorbed molecules. These include measurements of dispersed fluorescence from electronically excited molecules produced by UV dissociation of polymers,[23] translational energies of Ag, Cl, and AgCl emitted from AgCl surfaces,[24,25] translational energies of desorbed molecules, and photofragments following excitation of condensed films of H_2O and NH_3,[26] H_2S, and CH_3Br physisorbed on LiF,[27,28] or CH_3Br on Ni(111),[29] and CS_2 from CO_2 solid.[30]

Several of these systems involve direct excitation to repulsive potential surfaces leading to prompt photodissociation and desorption. Comparisons of adsorbate photodissociation to that in the gas phase have suggested ways in which photofragment energies are modified by kinetic or electronic interaction with different substrates. Following UV photodissociation of CH_3Br adsorbed on a LiF surface, Bourdon *et al.* observed desorption of CH_3 radical.[27] The CH_3 TOFs are similar to those from the gas phase dissociation but extend to higher energy than allowed by conservation of momentum for an isolated molecule. Results were explained with a dissociation mechanism operating on the same intramolecular potential as for gas phase CH_3Br, but with a higher effective mass for Br due to interaction with the surface. The translational energy of the methyl fragment shows little accommodation with the surface, the surface mainly changes the kinematics of the repulsive separation of Br and methyl.

Marsh *et al.* looked at the same reaction on a metal substrate.[29] UV photofragmentation of CH_3Br on Ni(111) should involve the same direct repulsive surface as in the work on LiF described above, but the TOF distributions of desorbed CH_3 fragments are different, much lower in energy. Energy loss may be occurring via electronic interaction with the metal. Image dipole coupling to a metal surface is important in electronic and vibrational relaxation of adsorbates, but may be too slow to be important here.[31] The UV excited CH_3Br has enough energy to access charge transfer

states a few eV above the ground state, which then lose energy to the metal. Charge transfer mechanisms such as the transient negative ion states proposed by Gadzuk[32] have recently been invoked in several experiments. Vibrational excitation observed following low energy collisions of NO with Ag(111) cannot be explained kinematically, but may be a result of charge transfer.[33]

3. Model systems

To bridge the gap between photodissociation of isolated adsorbates on well characterized surfaces, and etching of polymer films or biological tissues, we might study a series of increasingly complex model systems. Ideally, we would start with an isolated molecule, then see how its photochemistry is modified and new energy flow pathways opened by condensation and the presence of the substrate. The interpretation of surface experiments can be guided by the spectroscopy, photochemistry, and energy transfer properties of the excited molecule under progressively stronger interactions with surrounding species. Relevant information may be obtained from gas phase, matrix isolation, or neat molecular solid work. At this stage of our understanding, films of weakly bound molecular and physisorbed materials should be especially fruitful model systems.

To this end we have studied resonant UV photodesorption from a molecular film of nitric oxide. Condensed NO is a particularly interesting system: the solid is known to be completely dimerized, and the dimer bond strength is intermediate between values typical of van der Waals and covalent bonds. The gas phase spectroscopy of NO monomer, the only significant desorption product, is well understood, allowing product internal energy distributions to be determined. We will discuss the use of high-resolution time-of-flight spectra and resonance enhanced multiphoton ionization spectra to distinguish thermal from nonthermal mechanisms. We observed bimodal velocity distributions which give unambiguous evidence for two different desorption channels. The yield of each component of the bimodal velocity distribution varied independently as a function of laser wavelength, pulse energy, and film thickness. We interpret one peak as thermal in origin, and the other as resulting from a single photon, nonthermal photochemical desorption process. We will consider in detail the nonthermal channel's response to film and laser characteristics, its translational and internal energy distributions, and discuss possible desorption mechanisms.

II. EXPERIMENTAL

A film of 1–2000 ML of NO condensed on a Ag(111) substrate under UHV conditions at 25–50 K was irradiated at glancing incidence by 5 ns pulses of 220–270 nm laser light (4.6–5.5 eV) with 0.5–5 mJ/cm^2 power density at the surface. Translational energies of desorbed molecules were measured from time-of-flight (TOF) spectra taken with a mass spectrometer, while the internal energy distribution of desorbed molecules was determined by (1 + 1) resonance enhanced multiphoton ionization (REMPI) using the same laser and a microchannel plate ion detector.

Details of the UHV chamber, molecular beam, mass spectrometer, and substrate have been described previously.[34,35] Figure 1 is a schematic view of the apparatus. A bakeable stainless steel UHV chamber contained the single crystal substrate, liquid helium cold tip and crystal manipulator, sputter ion gun, Auger spectrometer, quadrupole mass

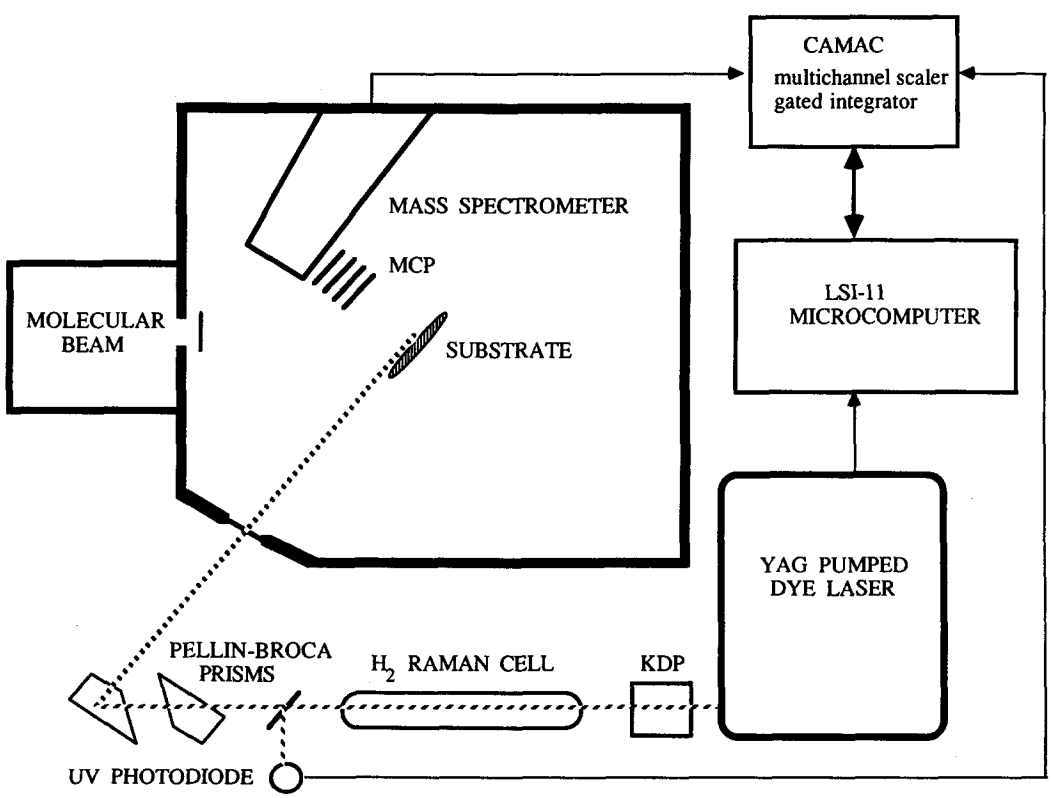

FIG. 1. Apparatus schematic. NO dosed from a molecular beam condensed on a liquid He cooled substrate. The NO film was excited by a tunable UV laser. Desorbed NO was detected by a quadrupole mass spectrometer, or resonantly ionized by the laser and detected with a microchannel plate.

spectrometer, and microchannel plate. The chamber was pumped by a 400 l/s ion pump and by the liquid helium cooled portions of the manipulator. Base pressure was $< 1 \times 10^{-10}$ Torr as determined by a nude ion gauge.

The substrate was a liquid helium cooled Ag(111) crystal. Defects and details of the substrate surface structure did not influence results of experiments with multilayer condensed NO. A chromel–alumel thermocouple was press fitted to the back of the crystal. The thermocouple was calibrated by comparison to known temperatures for bilayer Ar desorption and bulk Ar and NO desorption temperatures deduced from known vapor pressures.[36] We estimated the temperature calibration to be good to $\pm$ 5 K. When a rare gas layer was deposited on the Ag substrate and irradiated by the laser under conditions which would desorb NO, no rare gas desorbed. This clearly ruled out direct laser heating of the metal as a cause of fast peak desorption.

The first step in the experimental procedure was to dose the cold substrate with a molecular beam of NO to condense a thin film of NO solid. Photoelectron spectra of NO on Ag(111),[37] UV spectra of thin NO films[38] and x-ray diffraction[39] experiments indicate complete dimerization of NO in the solid.

A molecular beam source was attached to the main chamber. Two molecular beams could be used to dose the crystal. The center beam, used with NO or rare gases, has a diameter of about 1.25 mm at the crystal, and an angle of incidence of 45° from surface normal. The resulting dosed spot on the crystal was elliptical with a 1.25 mm minor axis and a 1.75 mm major axis. The rare gas flux with 20 psia backing pressure was about 0.56 ± 0.1 ML/s. The NO flux with 10 psia backing pressure was about 0.45 ± 0.1 ML/s. The side beam, used for rare gases, has a diameter of about 2.5 mm at the crystal and is incident at 43°. The dosed spot was an ellipse with 3.4 mm major and 2.5 mm minor axes. The rare gas flux on the crystal with a 6 psia backing pressure was 0.023 ML/s. We calibrated the fluxes by the dosing time required to produce features in thermal desorption spectra corresponding to monolayer, bilayer and bulk rare gas[36] or monolayer and bulk NO.[37] Sticking probabilities at 25 K were near unity. Dose times in coverage dependence experiments were controlled by a manually or timer actuated electromechanical beam shutter. The surface was continuously dosed with NO while taking most REMPI spectra. Kr and Ar gas were 99.995% pure from Cryogenic Rare Gas Laboratories or Liquid Carbonic. NO was C.P. 99% grade from Matheson.

A Quanta-Ray DCR-1 Nd^{+3}-YAG laser producing 5 ns pulses at 10 Hz pumped a PDL-1 dye laser containing Fluorescein 548. Wavelength was incremented by a stepping motor controller with a custom CAMAC interface. The typical wavelength increment was 0.025 Å (0.4 cm^{-1}). The dye laser output was doubled in a KDP crystal with servo-controlled angle tuning. A 50 cm focal length S1 grade quartz plano-convex lens focused the light in the center of a 120–230 psia H_2 Raman cell. After recollimation by a second identical lens, the fundamental, doubled or various anti-Stokes orders of the doubled light were selected by adjusting the angle of a dispersing quartz Pellin–Broca prism. A second Pellin–Broca prism with a mirror image orientation relative to the first was 63 cm away, followed by a 90° turning prism 2.4 m away at the UHV chamber. Finally, an adjustable entrance lens focused the laser through a Suprasil UHV window to the crystal 68–73 cm away. The laser beam entered along the axis of rotation of the crystal and detector and struck the crystal surface at a grazing 2 ± 1° angle of incidence, perpendicular to the center dosing beam. The laser polarization was 45° with respect to crystal normal, parallel to the dosing beam.

We aligned the laser by directing visible radiation through two beam defining apertures. The entrance lens was adjusted so that the visible light was focused on the portion of the crystal to be dosed with NO. The desired UV beam was then selected and directed through the two alignment apertures. Small entrance lens adjustments were usually required before a scattered light signal from the microchannel plate indicated that the UV beam was striking the crystal surface.

As wavelength varied, the dual Pellin–Broca prisms prevented a change in beam direction due to dispersion, but the angular shift between the two prisms caused beam walk at the entrance lens. Since the crystal was not exactly at the focal point of the lens there was some translation of the spot. The microchannel plate signal due to light scattered from the edge of the crystal did show a wavelength dependent change. The position change was 50–75 μm for a 500 cm^{-1} wavelength scan, smaller than the beam spot size. No variation in desorbed NO yield was detected with the mass spectrometer during such a scan, nor was there a change in REMPI intensity if the crystal was translated to compensate for beam walk.

By tuning the *same laser* used to excite the condensed NO film, we obtained REMPI spectra to measure the internal energies of NO monomer desorbed during the 5–10 ns laser pulse. All of the desorbed molecules remain within the laser beam during the laser pulse since the 5 μm travel distance of molecules in 5 ns was small compared to the laser beam diameter. We could use one laser because the solid optical absorption was broad, with a 12 000 cm^{-1} FWHM.[40] The absorption intensity of the solid changes by less than 10% for a typical 2445–2480 Å REMPI spectrum and need not be deconvoluted from the product spectra.

We used the doubled dye output for experiments near 273.7 nm. A 75 cm quartz or 61 cm CaF_2 entrance lens produced a laser beam cross section of about 0.8 mm diam. Maximum energy in a 5 ns pulse was about 1 mJ. Because of the grazing incidence angle, this corresponded to about 5 mJ/cm^2 or 1 MW/cm^2 power density at the NO surface. Pulse energies were determined from the average power of the 10 Hz laser, measured with a Scientech 38-0101 power meter. Spot sizes, and the resulting power densities, were estimated to within a factor of 3.

We used the second anti-Stokes Raman shift of doubled Fluorescein 548 dye output, around 223.85 nm, to obtain spectra of the NO $A\,^2\Sigma^+ \leftarrow X\,^2\Pi\ \gamma(1\text{–}1)$ band. Spectra show that the linewidth was about 1.2 cm^{-1}. A 75 cm nominal focal length quartz entrance lens produced a focal point 1.7 cm from the condensed NO for a beam cross section of

700×400 μm. A 150 μJ pulse resulted in a power density about 0.4 MW/cm^2 at the surface.

Our best spectra were of the γ(0–2) band near 247.2 nm, using light from the first anti-Stokes Raman shift of the dye. The 75 cm quartz entrance lens focused 4.5 cm from the sample for a cross section of 1000×300 μm. Pulse energy of 110 μJ produced a power density of 0.25 MW/cm^2 on the surface. This was typical for fast peak measurements.

We calculated laser absorption based on an analytic solution to Maxwell's equations. The model system was a three layer sandwich with both ends semi-infinite. Plane wave solutions were assumed in each region and matched at the boundaries to give Fresnel coefficients.These were then summed to give the electric and magnetic fields in each region, which yield the Poynting vector and power deposition in the medium.[40,41] The calculation indicated that $\approx 90\%$ of the incident light was reflected at the surface of the film.

The spectra must be normalized for variation of laser intensity. The power dependence of gas phase NO REMPI spectra was used to separate the desorption and ionization steps. We examined the REMPI signal from NO in the rotationally cooled dosing beam as a function of laser pulse energy for the $Q_{11} + P_{21}$ bandhead of the $A \leftarrow X$ (0–0) band. At low pulse energies, neither the $A \leftarrow X$ nor the $NO^+ \leftarrow A$ transition were saturated and the signal varied as P^2, where P was the laser pulse energy. After saturation of the $A \leftarrow X$ transition, the $NO^+ \leftarrow A$ transition remained unsaturated and the REMPI signal was approximately linear with laser pulse energy. The laser power density was sufficient to saturate the NO $A\,^2\Sigma^+ \leftarrow X\,^2\Pi$ bound to bound transition, but not to saturate the weaker $NO^+ \leftarrow A\,^2\Sigma^+$ bound to free ionizing transition.

Few isolated rotational lines were resolved because the Raman shifted laser linewidth was broad, 2.5 cm^{-1} (0.15 Å), and because a high rotational temperature produced a dense spectrum. Rotational populations were extracted from spectra with a nonlinear least squares fitting program. The intrinsic line strength of completely saturated lines was $(2J'' + 1)$ rather than the Hönl–London factors generally used for unsaturated lines. The data did not warrant more sophisticated treatments of partial saturation and intermediate state alignment.[42,43] The fitting program returned P_{mj}, a number proportional to the population of each M_J state. Initial fits allowing separate lambda state populations showed no detectable difference. They were assumed equivalent for final fits. A Boltzmann plot of $\ln P_{mJ}$ vs $E_{J\Omega}$, the rotational energy plus electron spin energy of a molecule with quantum numbers J and Ω, is linear with a slope of $-1/kT$ if the populations follow a Boltzmann distribution. A linear Boltzmann plot with a 297 ± 10 K temperature derived from the (0–0) band spectrum of 5×10^{-5} Torr of NO backfilled into the room temperature main chamber verified the accuracy of the fitting procedure.

Ions were detected with a modified Galileo FTD 2001 microchannel plate (MCP) mounted parallel to and 3.4 cm away from the Ag crystal. We substituted a flat plate anode for the impedance matched anode supplied by Galileo and added a collection grid above the active face of the MCP. The grid kept the ion collection potential constant when plate gain was varied. A collection grid voltage of 1360 V resulted in a 650 ns flight time between generation and collection of NO^+ ions. No signal from other ions was observed, but both NO^+ ions and scattered laser light produced MCP signal. To maintain linearity, we had to keep plate gain low enough to insure that individual channels did not saturate. The optimum gain was determined by comparing the large ion and scattered light signals with a small signal from a Hg lamp. The onset of saturation appeared as a decrease in ion or scattered light signal relative to that predicted from the small signal gain. The plate was operated at gain a factor of 2 or more below saturation of either scattered light or ion signal.

After the laser pulse, the time-of-flight of desorbed neutral molecules from the crystal to the ionizer of the mass spectrometer gave their translational energies. Desorbed molecules were electron impact ionized, mass selected (usually for NO monomer) and counted with a doubly differentially ion pumped extranuclear quadrupole mass spectrometer with a venetian blind electron multiplier. The mass spectrometer could be rotated from crystal normal to 90°, or from 45° to 90° with respect to the laser polarization. The detector had 1° angular resolution and viewed a 2.5 mm spot on the crystal at normal. The electron impact ionizer was 14.45 cm from the crystal, with an active ionizer length of less than 2 mm, providing a time resolution better than 2%. Typically TOF spectra of 200–10 000 laser shots were averaged. Backgrounds were on the order of 0.01 counts/shot/channel, and signal-to-noise ratios (S/N) for TOF spectra of the fast peak were typically about 100, ranging from 2 for desorption from monolayer coverage to 200 or better. S/N for conditions where the slow peak dominates was often > 1000.

Data acquisition was controlled by an LSI-11/23 Charles River Data Systems minicomputer interfaced to the experiment via a Kinetic Systems CAMAC controller. A custom multichannel scaler was used to acquire TOF spectra. Typical dwell time was 4 μs/channel. The laser Q-switch output was the zero time reference. For REMPI spectra we measured laser intensity, microchannel plate signal and baseline for each laser shot. Signals were acquired with a LeCroy 2249SG gated integrator. The integrator was gated to separate the MCP ion counts from scattered light and background signals. The 50 ns gates were produced by a KGE custom delay generator triggered by the laser Q-switch output. For laser energy measurement, a quartz beamsplitter plate directed a portion of the laser pulse through ND filters and a ground quartz diffuser into a 22 V reverse biased UV sensitive EGG UV100BQ photodiode. The diode signal passed through a custom analog integrator before reaching the LeCroy gated integrator. Typically 100–200 shots were averaged before the computer incremented the dye laser for the next point in the spectrum.

III. RESULTS

A. TOF spectra

We measured time-of-flight (TOF) spectra of photodesorbed NO monomer at several angles and as a function of

laser wavelength, laser pulse energy, NO layer thickness, distance of a supported NO layer from the underlying silver substrate, and substrate temperature. The raw TOF data were fitted, then transformed to differential flux vs time, velocity and energy, or integrated to give total desorption yields.

By varying experimental conditions, we could see two distinct, characteristic TOF patterns which we described as the slow and fast TOF peaks. The fast peak had a flux-weighted mean translational energy at normal $\langle E_T \rangle = 0.22$ eV, and could not be fitted with a single Maxwell–Boltzmann velocity distribution, while the slow peak was Maxwellian with $\langle E_T \rangle \leqslant 0.06$ eV. Under most of our experimental conditions only the fast peak was easily observable, but for thick NO layers and high laser fluences, the slow peak would appear.

Figure 2 consists of three flux-weighted TOF spectra which clearly show the fast peak, slow peak, and both together. The fast peak is shown in the top part of Fig. 2. Only the fast peak was present with thin films or low laser power, where desorption yields were low. Yield was about 2×10^{-3} ML/shot. At higher desorption yields, the slow peak appeared. A bimodal TOF spectrum for conditions where both fast and slow peas were present is shown the in middle part of Fig. 2. Yield was 6.3×10^{-3} ML/shot. The bottom of Fig. 2 shows the slow peak, which dominated for NO films thicker than 150 layers with 273.7 nm light fluences $\geqslant 3$ mJ/cm^2 of NO surface. Under these conditions desorption yield was one tenth of a layer or more per laser shot.

The fast peak was non-Maxwellian—broader in velocity than a single Maxwellian with the same peak velocity, and with an angular distribution sharper than cosine. We were able to fit the fast peak with a sum of two Maxwell–Boltzmann distributions at fixed temperatures, but with variable amplitudes and angular dependencies. "Temperature" is used here only as a convenient parameter to describe the fitting functions, which we will call the "high energy term" and "low energy term" of the fast peak fit. The fixed temperatures of 1925 K for the high energy term and 525 K for the low energy term were determined by fitting high S/N TOF spectra. A typical relative yield of high to low energy terms in the fast peak, measured along the crystal normal, was 1.8:1. *Again, this sum of Maxwellian terms chosen arbitrarily as a fitting function to describe the shape of the fast peak, and is not meant to imply that we have identifed components within the peak.* The data analysis and fitting procedures are described in the Appendix.

The fast peak did not change shape for photon energies from 4.6 to 5.6 eV, laser pulse energies ranging over a factor of 3, or varying NO layer thicknesses above 20 layers. Our sensitivity to changes in shape can be estimated from counting statistics. If the translational energy of desorbed molecules was proportional to photon energy, we would expect a maximum change of 50 meV in translation as the photon energy changed from 4.6 to 5.6 eV. That would be approximately equal to a 10 channel shift in TOF peak position, which corresponds to a 2σ uncertainty in counts, and should be evident. We therefore consider it probable, but not certain, that there was no change in the velocity distribution with changes in excitation wavelength. This will be important when we discuss possible desorption mechanisms.

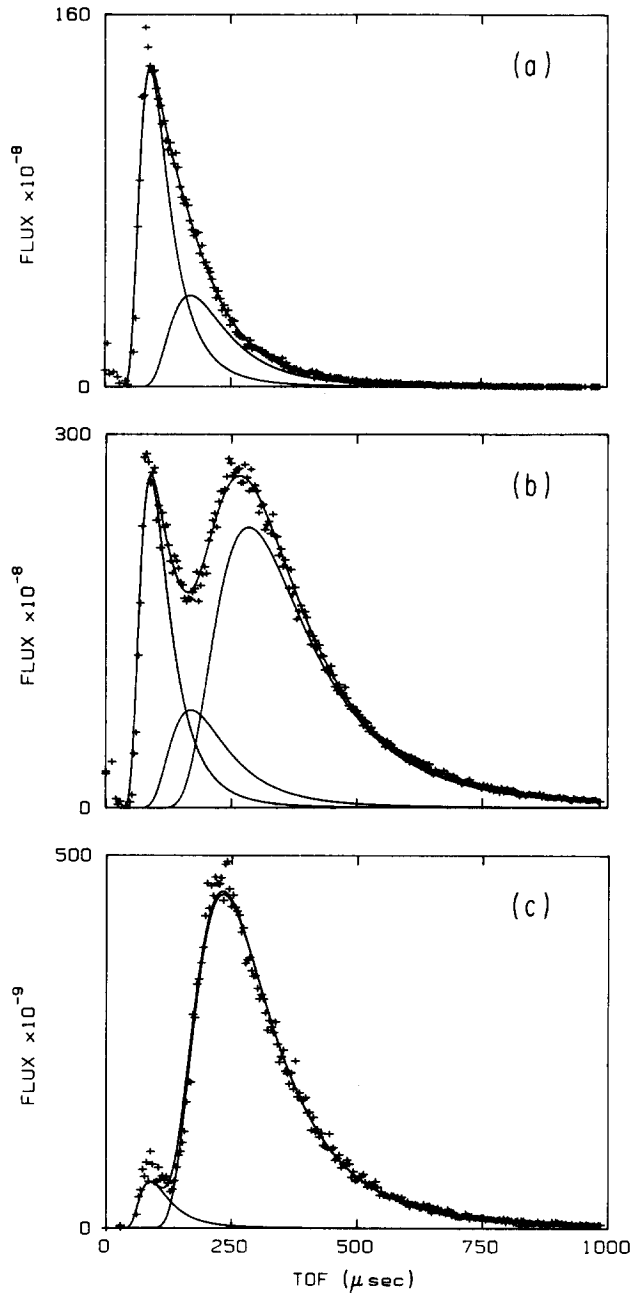

FIG. 2. Flux-weighted TOF spectra of NO monomer desorbed from a 250 ML film. The detector was at crystal normal. The laser pulse was 5 ns at a 10 Hz repetition rate. There were 255 channels of 4 μs width. (a) Fast peak. The laser wavelength was 247.4 nm with a fluence of 1.6 mJ/cm^2/pulse on a 0.3 mm^2 NO area. Total yield was about 1.2×10^{10} molecules/shot or 2×10^{-3} ML/shot. The fit is a sum of two Maxwellians at 1925 and 525 K in a ratio of 1.8:1. (b) Bimodal TOF spectrum. Wavelength was 273.7 nm with 3.5 mJ/cm^2 on an NO spot approximately 1 mm^2. There are about 1200 counts in the peak channel for a total yield of 1.0×10^{11} molecules/laser shot. The fit is a sum of three Maxwellian velocity distributions, the fast peak is 1925 and 525 K in 1.8:1 ratio, the slow peak is a single Maxwellian at 186 K. (c) Slow peak fit by a single Maxwellian distribution at 280 K. Laser was at 273.7 nm and 5 mJ/cm^2 on a 1 mm^2 spot. The total yield is about 1.4×10^{12} molecules/shot.

At low NO coverages, or when we changed the substrate temperature, the fast peak did change shape. We could ade-

quately describe the shapes by a change in the relative ratio of the two terms in the fitting function, without changing the "temperatures" of the terms.

Time-of-flight spectra as a function of desorption angle showed that yield from the slow peak, and each term used to fit the fast peak, had a different angular dependence, with the higher energy terms peaked more sharply toward crystal normal. Figure 3(a) shows flux-weighted TOF spectra at 0°, 35°, 65°, and 80° from crystal normal. The slow peak accounted for a quarter of total yield in these measurements; it was obscured at normal, but became more visible at large angles. Figure 3(b) shows the yield vs angle for each distribution used to fit the TOF spectra. The high and low energy terms of the fast peak could be fit with $\cos^4\theta$ and $\cos^2\theta$, respectively. The total fast peak yield had a $\cos^3\theta$ angular dependence. The slow peak was broader in angle than the fast peak, and was roughly cosine within large uncertainty. At 25°, the shape of the TOF spectrum does not change for a factor of 3 change in laser energy.

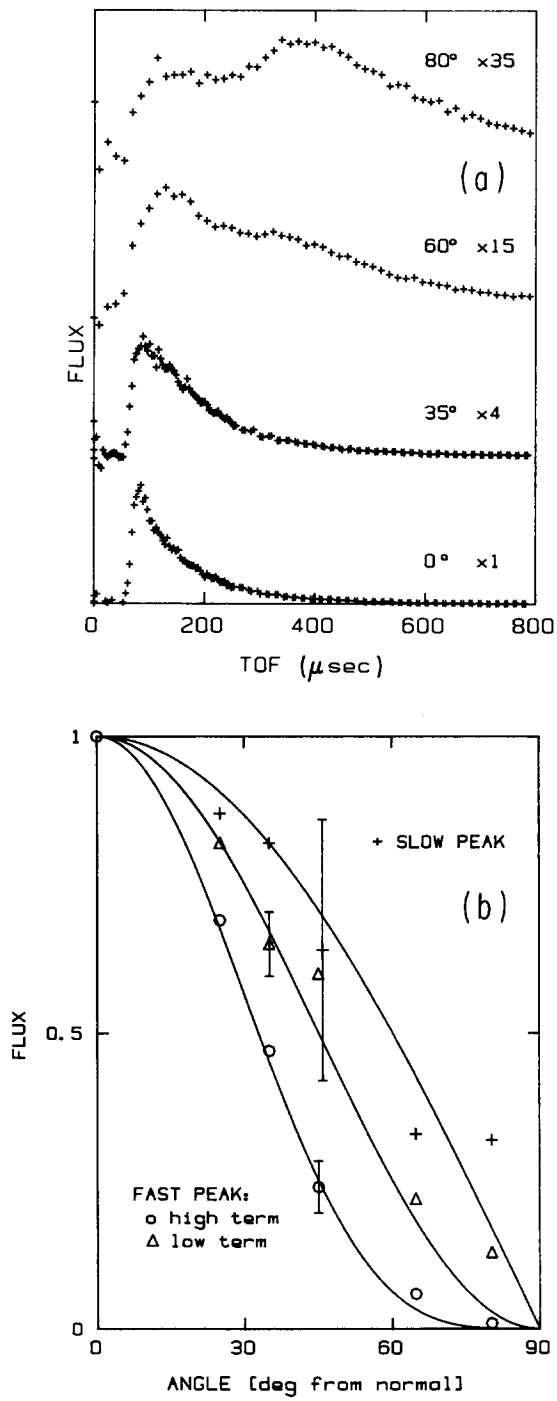

FIG. 3. Angle dependence of desorption flux. (a) TOFs at several angles from surface normal. The film thickness was ≥200 ML, the laser wavelength was 273.7 nm with a fluence of 1 mJ/cm². The slow peak was roughly cosine. The low and high energy terms in the fast peak fit were $\cos^2\theta$ and $\cos^4\theta$.

The average translational energy $\langle E_T \rangle$ of the fast peak calculated from the angular and TOF distributions in Eqs. (A5) and (A6) was 0.22 eV.

B. REMPI spectra

Rotational, vibrational, and electronic internal energy distributions of NO monomer desorbed during the 5–10 ns laser pulse were determined from (1 + 1)-REMPI spectra.

All REMPI spectra were taken with laser pulse energies several times higher than the $A \leftarrow X$ saturation point. The (0–2) and (1–3) band spectra were from NO desorbed during excitation of a continuously dosed thin film. A normalization factor of $1/E^{2.1}$ was determined from the REMPI signal as a function of laser pulse energy for the (1–3) bandhead, and for the $Q_{21}(21.5)$, and $R_{22}(20.5)$ rotational lines of the (0–2) band and for the (1–3) bandhead. The normalization was near quadratic because both the NO desorption step and the $NO^+ \leftarrow A$ step were linear in laser intensity while the $A \leftarrow X$ step is saturated. Pulse energies across a spectrum typically varied by less than about ± 50%.

REMPI spectra display features from vibrational and rotational states of the $^2\Pi_{1/2}$ and $^2\Pi_{3/2}$ ground electronic states of NO. Each of the two spin states have two nearly degenerate lambda states which label the orientation of the electronic orbital angular momentum with respect to the N–O bond. Part of the (0–2) band spectrum, normalized to laser pulse energy, is shown in Fig. 4 with the fit. A Boltzmann plot of P_{mJ} obtained from the REMPI spectra is presented in Fig. 5. The best line through the data gives a temperature of 2500 K, corresponding to an average rotational energy of desorbed NO of 0.24 eV per molecule.

Vibrational populations could be estimated when lines from more than one band were present in the spectrum. The (1–3) bandhead near 244.8 nm overlaps a portion of the (0–2) band spectrum as shown in Fig. 6. The relative vibrational population $v'' = 3 : v'' = 2$ is 0.85:1 assuming the $NO^+ \leftarrow A$ state transition strength is independent of A state vibrational quantum number and the $X(v'' = 3)$ state has the same rotational state distribution as the $v'' = 2$ state. The first assumption is reasonable because the NO A state is a Rydberg state: Franck–Condon factors for the $NO^+ \leftarrow A$ state transition should be approximately 1, independent of vibrational quantum number. A few weak spectral lines near 247.95 and 248.06 nm assigned to the (1–4) band were also detectable. An additional assumption of saturation of the (1–4) band $A \leftarrow X$ transition yields a 0.75:1 upper limit for the $v'' = 4 : v'' = 2$ population ratio. The $A \rightarrow X$ transition should be saturated because the Franck–Condon factor of

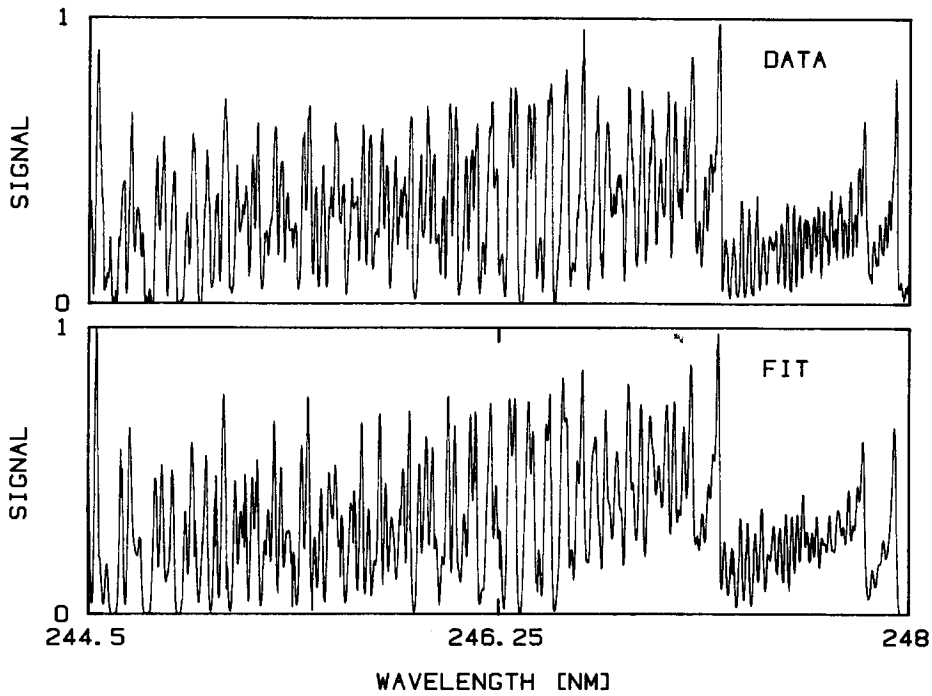

FIG. 4. REMPI NO $A(0) \leftarrow X(2)$ rotational spectrum. The film thickness was $\geqslant$200 ML, the laser wavelength was 244–270 nm with a fluence of 1.25 mJ/cm^2 on a 0.3 mm^2 NO spot. The fit was generated by nonlinear least squares on the set of rotational populations convoluted with calculated line positions.

0.135 compares favorably with the 0.237 and 0.069 of the (0–2) and (1–3) bands[44] which were shown to be saturated. Noisy spectra of the (1–1) band near 224.25 nm contained lines from the (0–0) band. The same assumptions as above yield 1.3:1 for the $v'' = 1$:$v'' = 0$ population ratio. Franck–Condon factors are 0.107 and 0.162 for the (1–1) and (0–0) bands. The REMPI spectra presented here can not relate the $v'' = 1$ and 0 populations to the $v'' = 2,3$ populations because spectra were not taken in a wavelength range where bands originating from $v'' = 1$ or 0 overlap bands originating from $v'' = 2,3$.

To estimate the average vibrational energy, we assume $v'' = 0$–3 are equally populated. Higher states may be populated, but the upper limit for the population of $v'' = 4$ is less than for $v'' = 3$. The average vibrational energy is then $\leqslant$0.4 eV.

The spin temperature cannot be well established, but may be cooler than rotations for $v'' = 2$. An estimate of 400–1100 K corresponds to a $\Omega = 3/2$:$\Omega = 1/2$ ratio of 0.9:1 and an average spin energy of desorbed NO of 0.006 eV.

We believe that the population sampled by REMPI is representative of molecules in the fast peak TOF distribution, although only those molecules desorbed during the 5 ns laser pulse can be observed. No slow peak was present when we took REMPI spectra. The power dependence of the REMPI (0,2) signal is approximately quadratic, consistent with the linear power dependence of the desorption that produces the fast TOF peak [Fig. 7(a)], combined with the saturated NO $A \leftarrow X$ transition and the linear $NO^+ \leftarrow$ NO A

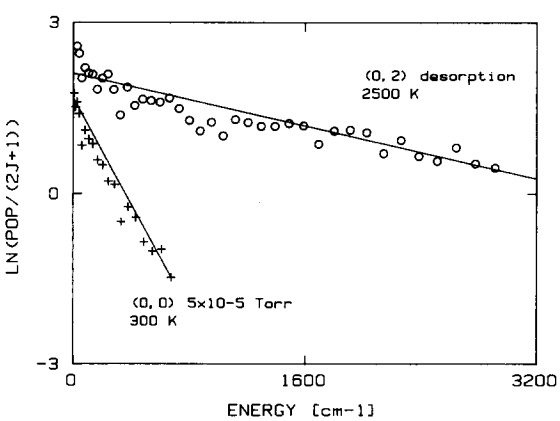

FIG. 5. Boltzmann plot of rotational distribution from the spectrum of Fig. 4. The best fit line is 2500 K. Also shown is a calibration run by filling the chamber with room temperature NO at 5×10^{-5} Torr.

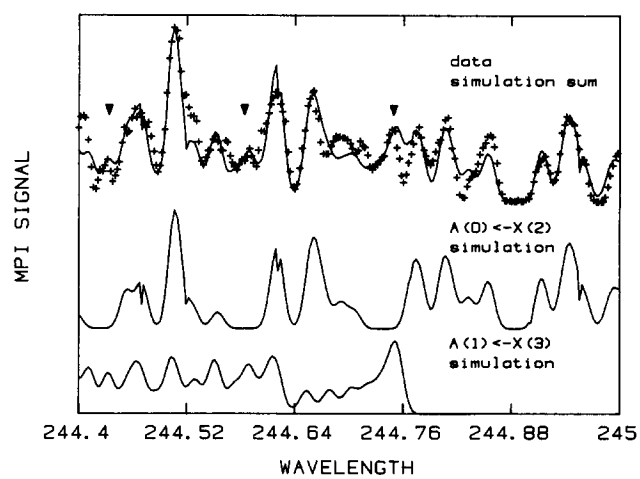

FIG. 6. Spectra showing vibrational excitation. The indicated peaks in the data are due to the $A(1) \rightarrow X(3)$ transition. The $v'' = 2$:$v'' = 3$ ratio is 1:0.85.

ionization step. The translational energy of selected rotational and vibrational states was not determined.

C. Yields and other results

1. Substrate heating

The Ag substrate did not heat significantly under typical conditions for NO fast peak desorption. Argon or xenon films of 2–10 ML at 25 K irradiated with 224–247 nm light between 0.2 and 3 mJ/cm^2 showed no desorption. Rare gas desorption is not seen from 2–5 ML Xe under thin 4–8 ML NO layers (Ag/Xe/NO), so there was little indirect heating of the substrate by transfer from the NO. Our calculations of light absorption indicate that rare gas over- and underlayers did not significantly affect the absorbance in the NO.

2. Desorbed species

The fast TOF peak consisted of NO X ($^2\Pi_{1/2}$ and $^2\Pi_{3/2}$) monomer. As our photon energy was usually below the threshold for the gas phase $A(0) \leftarrow X(0)$ transition, we would not expect to see electronically excited desorption products from a single photon process. Desorption in the A state would produce a nonresonant ion signal that would increase the base line of the REMPI spectra. The baseline of all REMPI spectra corresponds to no detectable ion signal. This gives an upper bound for desorption of NO monomer in the A state less than 0.05% of total desorbed NO.

With the mass spectrometer we looked for species other than NO monomer in the fast peak. Excitation of the NO film with about 1.2 mJ/cm^2 of light near 247.2 nm caused no detectable desorption of NO_2 or N_2O, which are possible products of photochemical reaction within the condensed NO. Upper bounds to desorption yields for NO_2 and N_2O were 1% and 3% of NO desorption yield, assuming ionization efficiencies similar to NO. Tuning the mass spectrometer to the $(NO)_2$ dimer at mass 60 revealed a signal less than 1% that of NO, but ionization cross sections and fragmentation probabilities for the dimer are not known. The dimer TOF peak did not coincide with the monomer fast peak. The dimer velocity was lower, and the maximum of the dimer TOF spectrum at a longer time than that of the monomer. We conclude that the NO fast peak does not arise from ionizer fragmentation of dimer, NO_2, or N_2O.

3. Laser power and wavelength dependence

The laser power dependence of desorption yield is very important in determining how many photons are required for desorption. Yield vs pulse energy is shown in Fig. 7. The fast peak was linear in laser pulse energy from 0.1–1.2 mJ/cm^2. The slow peak had a higher than linear dependence on laser pulse energy, which from 2.5–5.5 mJ/cm^2 could be fit by a single exponential. Figure 8 shows that the absolute yield in the fast peak at 3 wavelengths followed the NO solid optical absorbance spectrum.

4. Film thickness

Sow peak yield increased by a factor of 14 with an increase of layer thickness from 170 to 450 ML and the tem-

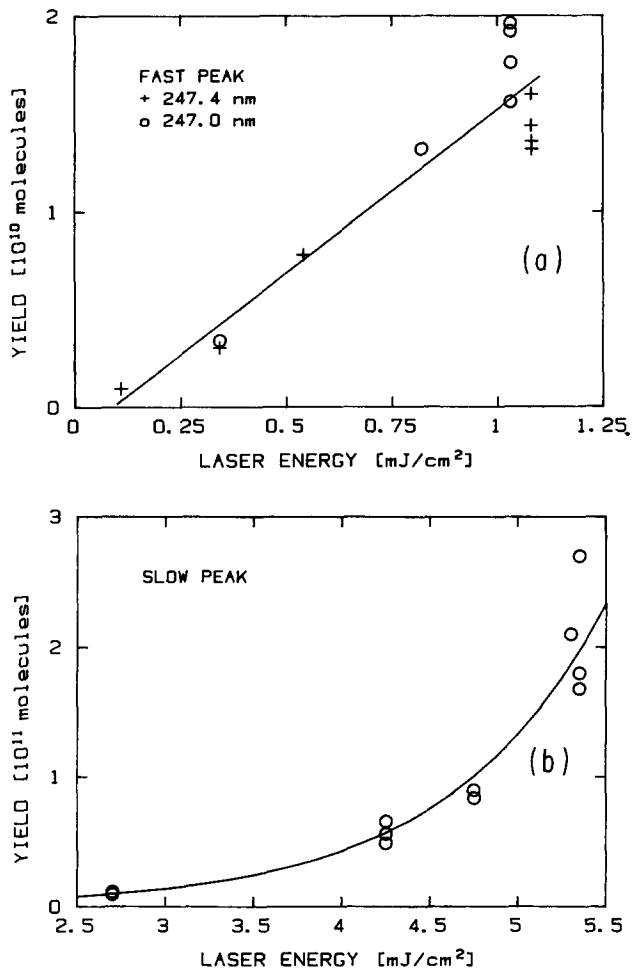

FIG. 7. Yield vs laser pulse energy. The NO film was 250 ML thick. (a) Fast peak. The laser wavelength was around 247 nm. (b) Slow peak. Laser wavelength was 273.7 nm.

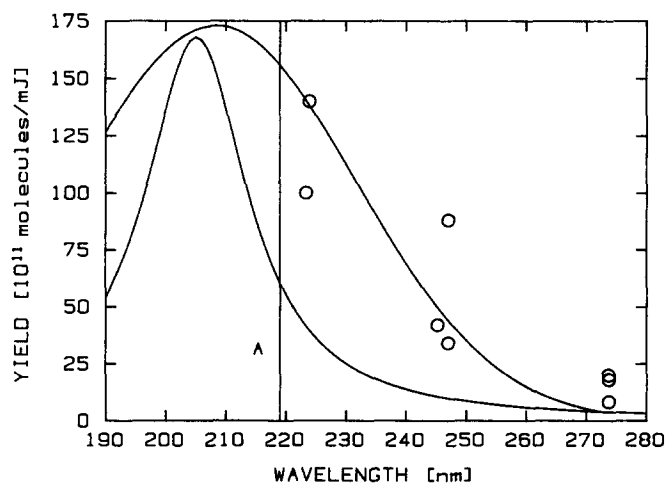

FIG. 8. Dimer and solid NO absorption spectra compared to the absolute yield of the fast TOF peak. Spectra are extrapolated from data in Refs. 38 and 58. The solid absorption was fit to a Gaussian and the sharper dimer spectrum to a Lorentzian curve. Normalization is arbitrary. The line "A" is the photon energy required to reach the gas phase A state threshold plus the binding energy of NO in the solid.

perature of the Maxwellian distribution increased by 30%.

The desorption yield in the fast peak as a function of NO layer thickness is shown in Fig. 9. Figure 9(a) the yield for low coverages from 1–5 ML, and Fig. 9(b) over a wider coverage range. Desorption yield increased by a factor of 2.5 as the NO thickness increased from 1 to 50 ML coverage, then saturated for NO coverages in excess of several hundred layers. The (0–2) band REMPI signal as a function of NO layer thickness is also shown in Fig. 9(b).

At low NO coverages, the shape of the fast peak changed, shifting to lower velocities. We can describe the peak shape by the ratio of the two terms in the fitting function. The relative magnitude of the high energy to low energy term decreased from its thick layer value of $\approx 2{:}1$. Below about 10 L the low energy term begins to dominate, the ratio is 1:2 near 5 L and at ≈ 1 ML doses only the low energy term appears, although the S/N is very poor and the coverage is not well known.

5. Rare gas over- and underlayers

Small amounts of rare gas deposited on top of the NO layer sharply reduced NO desorption. Figure 10(a) shows the NO yield attenuation vs argon overlayer thickness on 85 ML of NO on 10 ML of Ar (Ag/Ar/NO/Ar). The laser was tuned to 247 nm and produced a fluence of 1.3 mJ/cm^2 of NO surface. One layer of Ar attenuated 60% of NO desorption and a 2.4 ML Ar overlayer blocked 90% of the NO desorption. NO signal slowly recovered with irradiation time as the overlayer was depleted. After the laser was on for 75 s at 10 Hz, the NO signal increased to 60% of its value with no rare gas overlayer. A 1 ML krypton layer on 3 ML of NO on 3 ML of Kr, irradiated with 1.5 mJ/cm^2 of 246 nm light, showed initial attenuation of 80%. After 750 laser shots only half of the rare gas overlayer was left, and NO yield was back to 50% of its uncovered value.

Looking at the rare gas desorbed by exciting the underlying NO layer, we found that about 6×10^{-4} of a Kr monolayer per laser shot was removed. This was one tenth of the

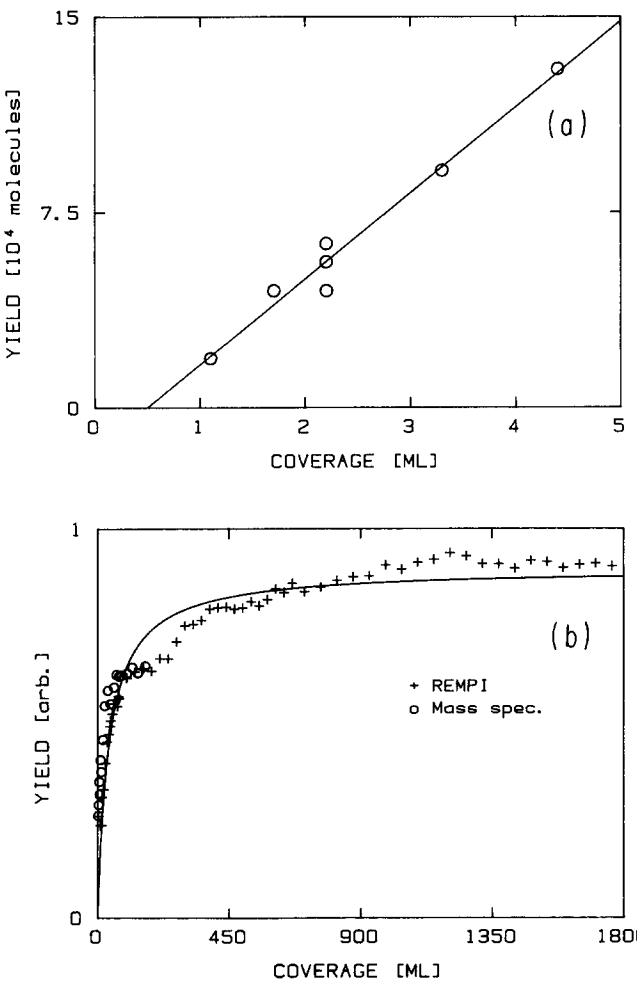

FIG. 9. Desorption yield vs NO layer thickness. Fast peak conditions: the laser wavelength was 247.4 nm with a fluence of 1.6 mJ/cm^2 on a 0.3 mm^2 NO spot. (a) Yield at low coverage. Absolute yields in molecules/laser shot from integrated mass spectrometer TOF data. (b) Higher coverages showing saturation. Both REMPI data from the (0–2) bandhead and mass spectra data are shown, arbitrarily scaled.

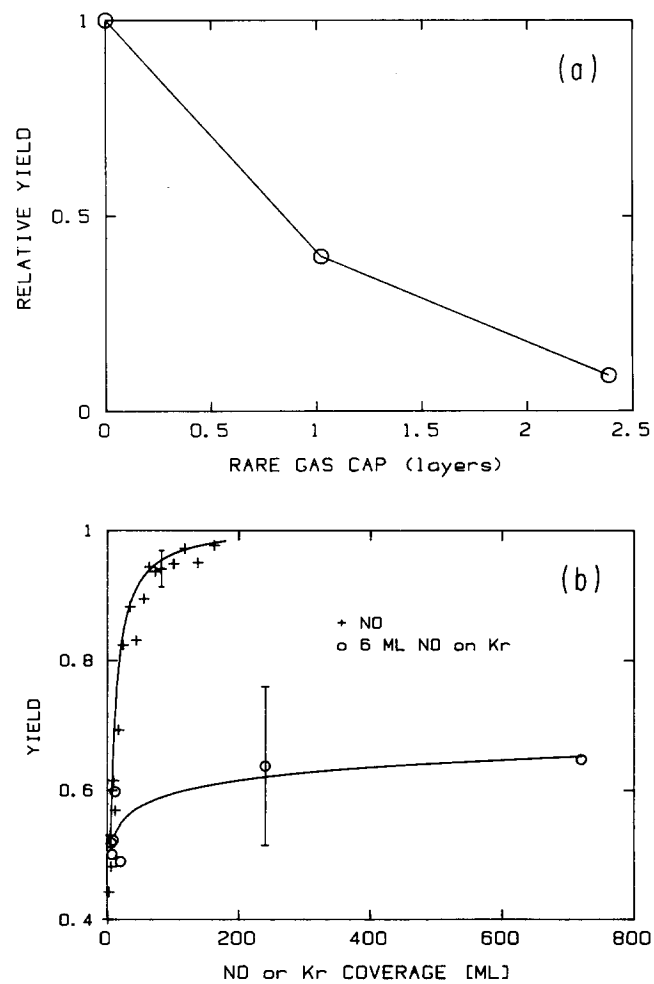

FIG. 10. Rare gas overlayers and underlayers. (a) Attenuation of NO desorption yield in the fast TOF peak by an argon overlayer. The irradiated film consisted of the Ar overlayer on 85 ML of NO on a 10 ML argon underlayer. The laser wavelength was 247 nm with 1.3 mJ/cm^2. (b) Yield vs distance to substrate. A variable Kr spacer thickness under 6 ML of NO. The NO layer thickness curve from Fig. 9 is also shown.

amount of NO that would be desorbed under similar conditions without an overlayer. A TOF of Ar desorbed from a 10 ML cap on 40 ML or more of NO, under conditions where only the fast NO peak would be seen, was fitted similarly to the NO fast peak TOF. The ratio of high to low energy terms was 0.85 ± 0.2, a somewhat colder distribution than the 1.8 ratio for the NO fast peak. Under conditions where 75% of total NO yield was in a 220 K slow peak, Kr overlayer desorption was fitted reasonably well with a single Maxwellian at 424 K.

We measured desorption yield as a function of the distance from the NO film to the metal substrate by placing a constant NO layer of 6 ML on top of a rare gas spacer of variable thickness, shown in Fig. 10(b). Yield from NO on Kr spacers thicker than 10 ML is less than for pure NO layers of similar thickness. Yield may be independent of distance from the NO surface to the metal substrate.

6. Substrate temperature

Figure 11(a) shows that yield in the slow peak increased strongly with substrate temperature: a factor of 400 gain in yield with a change in substrate temperature from 28 to 67 K. Increasing the substrate temperature had a smaller effect on the fast peak. Desorption from a 50 K substrate increased the fast peak yield at normal by a factor of 1.5 ± 0.2 relative to the 28 K substrate, and raised the high to low energy term ratio of the best fit to 3.8 ± 0.6 from 1.8. The angular dependence of the two terms in the fast peak fit is shown at two substrate temperatures in Fig. 11(b). When the substrate temperature was raised from 28 to 50 K, the low energy term still had a $\cos^2\theta$ distribution, but the high energy component sharpened to $\cos^7$ from $\cos^4\theta$. Annealing the NO layer or growing the layer at 50 K then reducing the temperature to 28 K increases the high to low energy term ratio to 2.7 from 1.8 at normal, but the total angle integrated yield does not increase relative to the unannealed film.

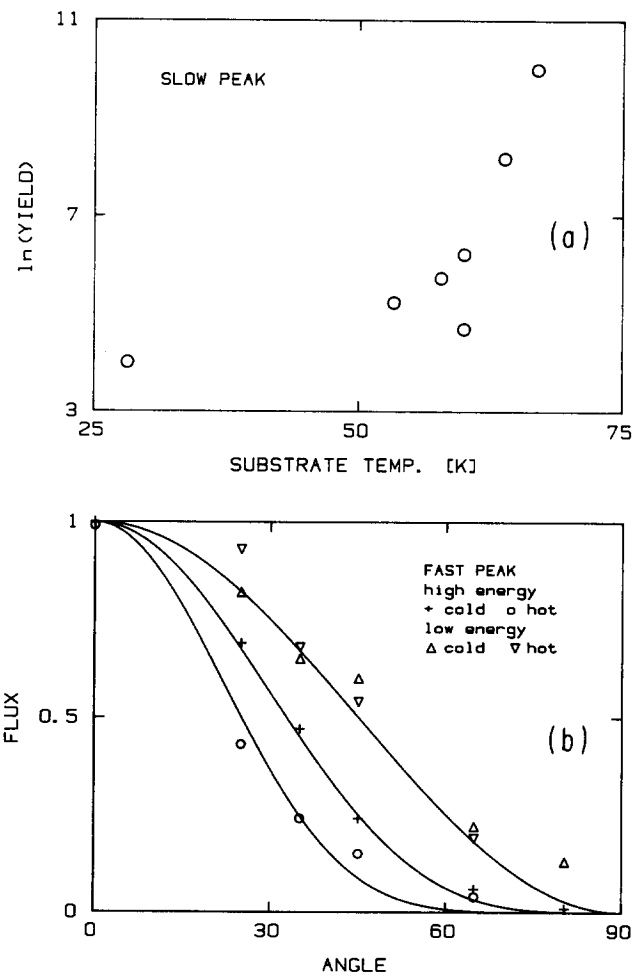

FIG. 11. Substrate temperature effects. (a) Temperature dependence of slow peak yield. The film thickness was 170 ML, the laser energy was 1 mJ/cm² at 273.7 nm. (b) TOF fast peak angular dependence vs surface temperature. The film thickness was >200 ML, the laser wavelength was 273.7 nm with a fluence of 1 mJ/cm². The low energy term remained $\cos^2\theta$ while the high energy term of the fast peak fit changed from $\cos^4\theta$ to $\cos^7\theta$.

7. Ablation and annealing

Fast peak yields were <0.005 ML per laser shot, too low to affect coverage during a run, but the much higher yields under conditions where the slow peak dominates can remove significant amounts of NO. Figure 12 shows yield vs coverage as thick layers ablate during irradiation after different initial dosing times with laser blocked. Since thicknesses could change rapidly over the course of a measurement, they were estimated at the midpoint of the interval using the dosing rate and measured desorption rate. Desorption yields are very high in the first few laser shots, followed by exponential decay of yield with decreasing coverage. The yields after burning down to equal coverages appear to vary with initial dose, but it is not clear if this shows annealing of the film, or is due to uncertainties in the effective laser spot size leading to errors in the calculated coverages.

D. Perturbations after desorption

Our TOF and REMPI spectra reflect the distribution of energy from the final interaction with the surface because

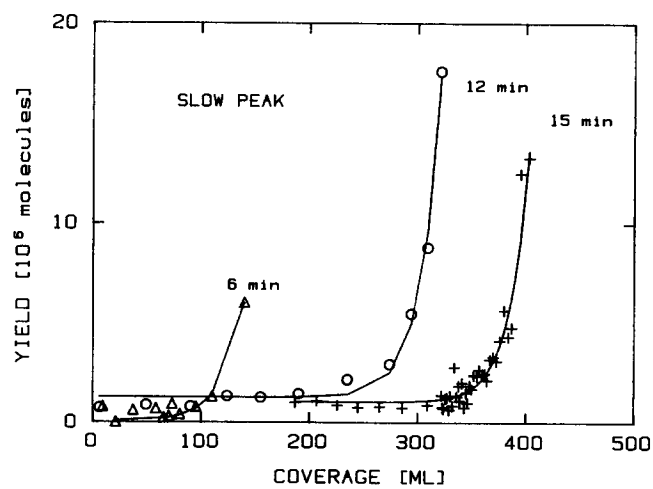

FIG. 12. Ablation. Yield vs coverage after initial doses with laser blocked. Doses of 6, 12, and 15 min correspond to initial coverages of 160, 325, and 400 ML before irradiation. There are 20 laser shots per point. Laser wavelength was 273.7 nm with a fluence of 4.5 mJ/cm² of NO surface in a 1 mm² spot. About 90% of the yield was in the slow peak.

the molecules were not perturbed in the gas phase following desorption. Collisions and nonresonant MPI plasma formation were not sufficient to affect the distributions. Due to surface disorder, some molecules may strike the surface again following desorption, but most will exhibit the nascent energy distribution from the initial desorption event.

1. Plasma formation

Plasma formation from nonresonant MPI was not significant in this experiment. Fluences were much lower than required for plasma formation in other cases where desorbed molecules had translational energies comparable to those we observed.[45–47] Threshold fluences for plasma formation with 248 nm light incident on Al_2O_3 are about 0.5 J/cm^2. Our fluences were $\approx$3–5 mJ/cm^2. Also, there was no change of NO translational energy with fluence as there was in one study involving plasma formation.[47]

2. Collisions

Collisions influenced the slow peak TOF distributions when the desorption yield was high. Assuming a cos θ angular distribution, a desorption yield of at least 1.8×10^{16} molecules/cm^2/shot from an $\approx$ 500 ML NO layer in 800×1250 μm or about 1 ML/shot was required for collisions to induce a slight broadening of the Maxwellian distribution as shown in Fig. 13(a). The development of supersonic flow in the slow peak is shown in Figs. 13(b) and 13(c). Note that the fast peak remains distinct.

Fast peak TOF spectra and REMPI rotational and vibrational distributions should not be affected by collisions in the gas phase. Experimental results in other systems with similar desorption yields suggest that collisions may slightly distort angular distributions, but not enough to account for the sharply peaked distributions we observed, nor for changes caused by annealing the NO layer.[3,5]

The collision probability is proportional to $N\sigma$, where N is the coverage desorbed and σ the collision cross section, with a weaker dependence on the temperature and pulse duration.[3] For a Maxwellian distribution at 1925 K, desorbing 3×10^{12} molecules/cm^2 from a 0.4 mm^2 spot (0.005 layers) in 5 ns, a 40 Å^2 cross section gives a maximum collision probability along normal of 5%. In fact, Fig. 13 shows the onset of collisional perturbation of the *slow* peak TOF distribution only near desorption of 1 ML/shot, which was 200 times greater than the typical yield in the fast peak. We do not see any change in shape of the fast peak as yield varies with laser energy.

Collisions have an even smaller influence on REMPI spectra. Because one laser was used to both desorb and detect molecules, only molecules desorbed in the first 5 ns are detected. During this time there is a less than 2% probability of a gas kinetic collision for desorption of 0.005 layers of NO. Rotational state changing collisions in NO have a cross section 1.5–2.5 times the collision cross section.[48,49] This value is too small to collisionally perturb REMPI spectra. Vibrational relaxation is even less likely with a cross section several thousand times lower than the collision cross section.[50]

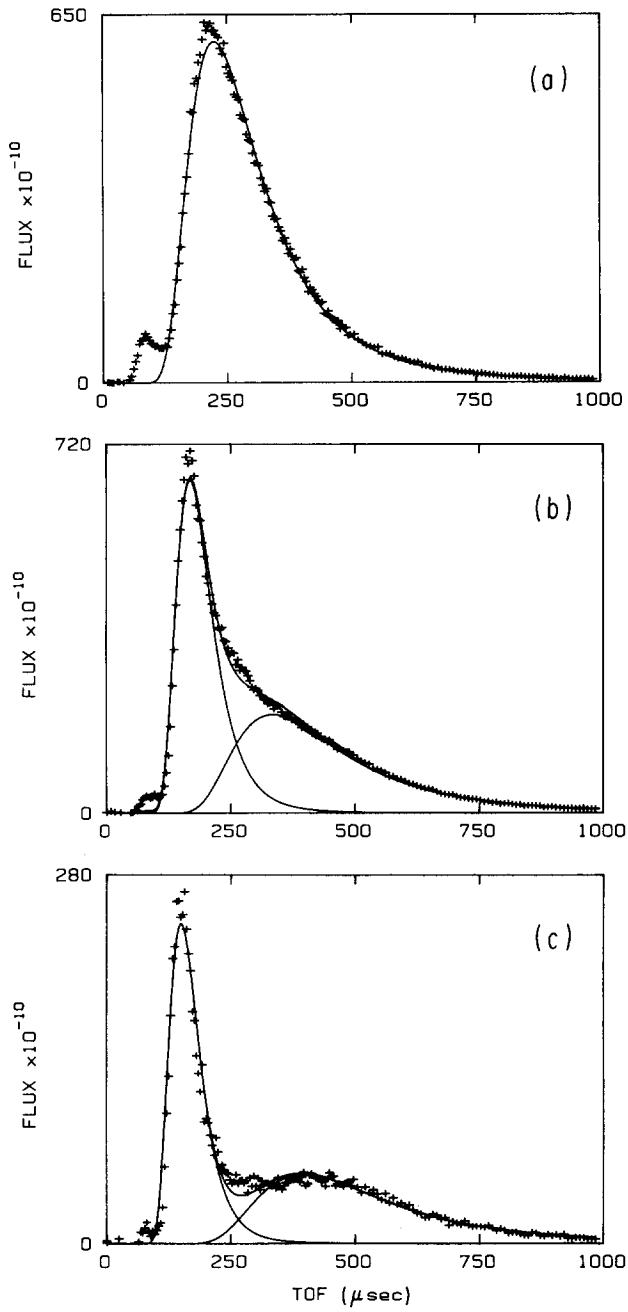

FIG. 13. Collisions in the slow peak. (a) Onset of collisional regime. Slow peak fit to a Maxwellian distribution at 300 K. The film thickness was > 400 layers, the laser wavelength was 273.7 nm with a fluence of 4.5 mJ/cm^2 of NO surface in a 1 mm^2 spot. The total yield is about 1.7×10^{13} molecules/shot, or 1.35×10^8 molecules/shot into $7.6\times10^{-5}\pi$ sr at normal. (b) Supersonic expansion. Note the fast peak is distinct from the supersonic peak. The fit consists of a Maxwellian at 135 K and a shifted Maxwellian at 150 K with a 62 000 cm/s stream velocity. The yield ratio of the two curves is 1:1.2. The supersonic peak has a speed ratio $S = 2.2$ and a Mach number $M = 2.5$. (c) The fit consists of an unshifted Maxwellian at 100 K and one at 170 K with a 71 000 cm/s stream velocity. The yield ratio is 1:1.1. $S = 2.3$, $M = 2.7$.

IV. DISCUSSION

The independent behavior of the two TOF peaks in this experiment implies at least two fundamentally different desorption mechanisms. We attribute the slow peak to laser induced thermal desorption (LITD) and the fast peak to

one or more nonthermal single photon desorption mechanisms.

The two mechanisms are most clearly distinguished by the dependence of yield on laser fluence and the energy distributions of desorbed molecules. For a single photon process, yield will be linear in fluence. Yield vs fluence for the fast peak, Fig. 7(a), is linear. For thermal desorption over a wide range of conditions, the laser induced temperature jump will be roughly linear in fluence. If the desorption rate follows an Arrhenius law, the result is an approximately exponential dependence of yield on fluence as in Fig. 7(b). Translational and internal energies for a thermal process will exhibit Boltzmann distributions. A nonthermal photochemical mechanism, however, may result in nonequilibrium energy distributions in desorbed molecules. We observed a Maxwell–Boltzmann velocity distribution for the slow peak and non-Boltzmann TOF and internal energy distributions in the fast peak. The measured desorption yields as a function of NO layer thickness and initial substrate temperature also assist in assigning mechanisms to the two peaks.

A. Slow peak

The slow TOF peak showed a Maxwellian velocity distribution, Figs. 2(c) and 13(a). We observed distributions with temperatures from 160 to 280 K. The angular distribution was broad, approximately cosine, as seen in Fig. 3(b). Yield increased strongly with NO layer thickness. Fig. 11(a) shows the sharp increase in yield as substrate temperature was increased. The yield vs laser fluence dependence of Fig. 7(b) can be fit with an exponential. These results are consistent with a laser induced thermal desorption (LITD) mechanism for the slow peak.

We restrict our use of the term "thermal desorption" to cases in which at least local thermal equilibration of the initial excitation precedes desorption. If temperature gradients are macroscopic and rates of heating slow compared to times for energy relaxation into all modes of neighboring molecules then the thermal diffusion equation:

$$\nabla^2 T = \frac{c\rho}{k}\frac{\delta T}{\delta t} - \frac{q}{k}, \tag{1}$$

where c is heat capacity, ρ density, k thermal conductivity, and q is the source density, is sufficient to describe the energy flow. Since there is complete conversion of the initial excitation into heat prior to desorption, the energy of the desorbed molecules is dependent only on the temperature profile at the surface at the time of desorption, and their yield on the time evolution of the surface temperature, independent of the heat source. For LITD, calculations of yield and temperature of desorbing molecules should depend only on the laser pulse intensity characteristics, film composition and dimensions, and thermal boundary conditions.

In spite of these restrictions, LITD can still exhibit nonequilibrium desorption characteristics. Even in conventional thermal desorption, microscopic reversibility requires desorbing molecules to have a Maxwellian velocity distribution at the surface temperature and a cosine angular distribution only if the sticking probability is independent of energy and incident angle. Conversely, although Maxwellian TOFs have been measured in a number of LITD experiments,[4,5,51] they do not unambiguously indicate the surface temperature. Brand and George have shown that a Gaussian surface temperature profile can still result in a single temperature Maxwellian velocity distribution for desorbing molecules.[52]

Nevertheless, since we expect the sticking probability to be unity at thermal energies for low temperature NO multilayers, and the laser spot size was large enough so that surface temperature should have been relatively uniform, the observed Maxwellian TOF velocity distribution and near cosine angular distribution do suggest thermal desorption.

The solution of the heat flow problem in laser absorption is discussed by Ready and others.[53,54] The time dependent temperature profile in our film might be modeled in one dimension, since the laser spot diameter was much greater than the film thickness, but it must take into account the detailed laser pulse characteristics and the light absorption depth profile. The energy of desorbing molecules should be included in the total energy balance. If there are phase transitions, there will be moving boundaries between solid, liquid, and vacuum. Calculation of the surface temperature is highly model dependent and sensitive to poorly known laser parameters, and will not be attempted. We will make qualitative arguments to show that our results are consistent with continuum heat flow and estimate desorption yield based on simple Arrhenius kinetics.

We estimate NO thermal properties from those of solid N_2 at 25 K[55]: thermal diffusivity $\kappa = 5\times10^{-3}$ cm^2/s, thermal conductivity $K = 3\times10^{-3}$ W/cm K, and density $\rho = 1.2$ g/cm^3. We assume film thicknesses of 3 Å per layer. For solid NO at low temperatures we have the heat capacity $C_p = 0.43 + 0.016T$ J/mol K and enthapy of sublimation $\Delta H_s = 3822 + 5.15T - 0.03T^2$ kcal/mol.[56] The thermal diffusion length is then on the order of 1000 Å for a 5 ns laser pulse.

The incident laser directly heated the adsorbed NO layer, but there was little heating of the underlying metal, as shown by the lack of desorption from rare gas films. Heat then flows from the NO film to the cold silver substrate. The deposited energy is efficiently transferred away by the silver, which is at least 10^4 times more thermally conductive than the condensed NO (single crystals may have thermal conductivities more than an order of magnitude higher than the pure polycrystalline metals). We can consider the metal to be fixed at 25 K. It is then reasonable to expect that the peak surface temperature increases with NO layer thickness, laser power or substrate temperature. We also expect an Arrhenius rate law to describe the desorption. If we suppose the surface temperature increases linearly with layer thickness, laser power or substrate temperature, yield should be roughly exponential in these factors. We saw that the yield vs laser fluence dependence of Fig. 7(b) can be fit with an exponential. Figure 11(a) shows a greater than exponential rise in yield as substrate temperature was increased, and yield also increased strongly with thickness.

Under typical experimental conditions—laser power $I = 1$ MW/cm^2, calculated reflectivity at glancing incidence 90%, substrate temperature $T_0 = 25$ K, film thickness 750

Å—the measured TOF of the desorbing molecules gave a temperature of 220 ± 60 K. Using this as the surface temperature, we estimate the yield expected from simple Arrhenius kinetics:

$$-d\theta/dt = \nu\theta e^{-\Delta H_s/kT}. \quad (2)$$

Surface density $\theta = 10^{15}$ cm^{-2}, a typical preexponential of $\nu = 10^{13}$ s^{-1}, enthalpy of sublimation $\Delta H = 4$ kcal/mol. We assume no adsorption barrier. At 250 K, a 0.5 mm^2 spot gives 2.5×10^{13} molecules per 5 ns laser shot. Measured yields were 10^{12}–10^{13} molecules/shot. Under these conditions we calculate 50 ergs/shot laser energy absorbed, and about 2 erg/shot in desorbed molecules.

At high yields, the layer thickness and possibly the structure of the film changed during the laser pulse. The decrease in yield as thick layers burn down over many laser shots is shown in Fig. 12. It is possible that the film anneals with heating. We know the initial NO dose, but we are uncertain of the area from which molecules are desorbed, so coverages following irradiation may be in error.

That the slow peak is due to thermal desorption is suggested by its Maxwellian TOF and broad angular distribution. That it is due to bulk heating of the NO layer is supported by the exponential dependence of yield on laser power, and the strong increase in yield with layer thickness and initial substrate temperature.

B. Fast peak

To undersand the origin of the fast peak, we look at product energy distributions to propose mechanisms, and desorption yields to learn something about the dynamics of energy flow between the excited moelcule and its surroundings. First we review the results. Then we comment on NO dimer spectroscopy and some possible desorption mechanisms, and consider excitation and modes and energy transfer pathways opened by condensation. Finally we attempt a general energy balance for photodesorption from the suface of a condensed film supported on a metal substrate.

Review of fast peak results: The fast TOF peak was present in all of our experiments, at laser wavelengths from 224 to 273 nm. It was most easily studied when the slow peak was small: with thin films (< 100 ML) or low laser energies (< 3 mJ/cm^2). NO monomer in the $^2\Pi$ electronic ground states was the dominant product. Some $(NO)_2$ dimer was seen, but there was no detectable N_2O or NO_2. The total yield was linear in laser pulse energy from 0.1 to 1.25 mJ/cm^2. The TOF distribution of the fast peak was non-Maxwellian and non-cosine, with $\langle E_T \rangle = 0.22$ eV. The shape of the TOF spectrum was not altered by changes in photon energy from 4.6–5.6 eV, or by varying laser power over an order of magnitude. For films less than 10 ML thick the peak shifted to lower energy. Increasing the substrate temperature or annealing the film moved the peak to higher energy, as measured at crystal normal, and the angular distribution sharpened. Total yield increased with NO layer thickness: desorption was seen from about 1 ML and yield increased rapidly to 50 ML and more slowly thereafter. A "cap" of 3–5 ML of argon on top of an NO film attenuated NO desorption by > 90%. Yields of NO on top of rare gas spacers of 10 ML or more show no dependence on distance from the substrate. The vibrational population ratio of $v = 3$ to $v = 2$ was 0.85, and higher vibrations were seen. Rotational spectra of $v = 2$ molecules give $T_R \approx 2500$ K.

1. Possible mechanisms

Several observations help to suggest desorption mechanisms for the fast peak. From the linear power dependence, desorption was shown to be a single photon process. Ground state NO monomer was the product. When we varied excitation wavelength, desorption yield followed the solid absorption spectrum. The translational energy distribution was invariant with excitation wavelength and film conditions. The internal energies were not in equilibrium: there was more energy in vibration than rotation or translation. We will consider a few processes consistent with these results.

a. NO dimer. Our films consisted of NO dimers. Photoelectron spectra of NO on Ag(111)[37], UV spectra of thin NO films,[38] and x-ray diffraction[39] experiments all indicate complete dimerization of NO in the solid. Figure 8 shows extrapolations of the UV absorption spectra of gas phase NO dimer and condensed NO solid. The dimer spectrum shows a peak near 200 nm, and a FWHM between 20 and 40 nm.[57,58] The breadth and lack of vibrational structure suggest that the excited dimer rapidly dissociates. The spectrum of condensed NO is broader and perhaps slightly red shifted with a peak at 210 nm and a FWHM of about 60 nm.[38] For most molecules that are gaseous at room temperature, the intramolecular potentials are not greatly affected by condensation,[59] so as a first approximation, we will consider the desorption as dissociation of an NO dimer. We sketch pseudo diatomic diagrams of a few dimer dissociation mechanisms in Fig. 14.

b. Direct dissociation. Direct dissociation of NO dimer by excitation to a repulsive surface correlating to electronically excited monomer, Fig. 14(a), is the first mechanism to consider. This process was seen in the gas phase by Carrasquillo.[60] Dispersed fluorescence from A and B state NO monomer following 206–214 nm excitation of NO dimers in a molecular beam shows that a portion of the NO dimer band results from excitation to repulsive regions of dimer electronic states correlating at large internuclear distance to one X state monomer and one A or B state monomer. In our experiments, such a process can be ruled out. Desorption of electronically excited states by a single photon was not possible. Excitation and desorption energetics prohibit direct repulsive desorption of the A or B states of NO from the solid for the 224–274 nm range of excitation wavelengths. Only wavelengths shorter than 219 nm can exceed the 123 kcal/mol energy needed to excite the NO monomer A state plus the 4 kcal/mol binding energy of ground state NO monomer in NO solid. Our REMPI base line was zero signal, verifying insignificant desorption of electronically excited states. Also, the $a\ ^4\Pi$ state is not accessible by a vertical transition below 6 eV, eliminating any possibility of its participation.

Although there are also dimer electronic states that correlate to two X state monomers,[61] direct photon absorption

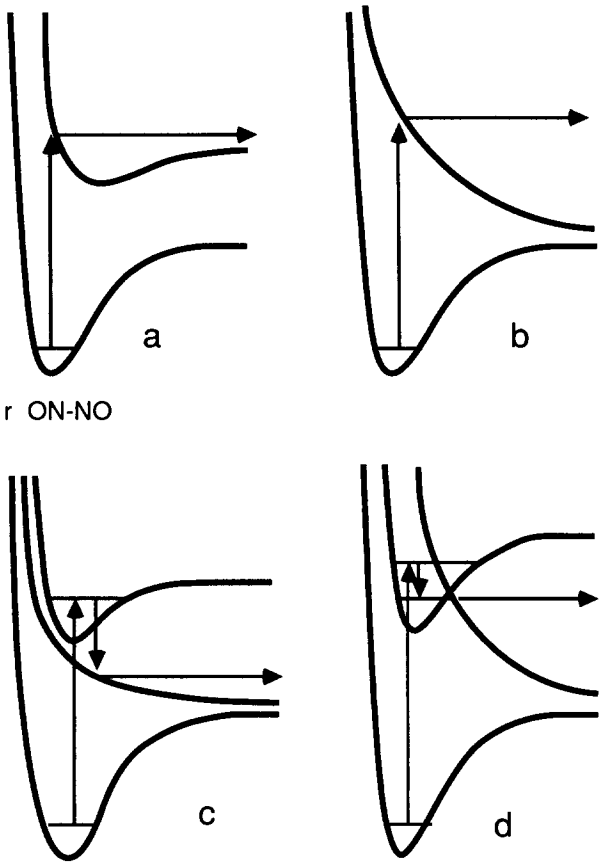

FIG. 14. Possible dimer photodissociation mechanisms. Pseudodiatomic diagrams of the N–N dimer bond with energies not to scale. (a) Direct dissociation to electronically excited products. (b) Direct dissociation to ground state product. (c) Radiative or Förster transition to ground state. (d) Upper state relaxation followed by internal conversion.

to a repulsive state, Fig. 14(b), seems unlikely. The translational energy of desorbed NO is far less than the photon energy, and does not vary with excitation wavelength. The *cis* structure of the NO dimer should cause rotational excitation during impulsive separation, and monomer rotations would be easily excited in collisions, but impulsive separation alone cannot account for the observed vibrational populations.[62]

c. Dissociation on the ground state surface. Internal conversion will result in dissociation on the ground state potential surface. NO monomer self-quenching studies of the A state suggest efficient internal conversion in NO dimer.[59] Quenching of NO(A) is thought to occur through a charge transfer intermediate, and the excited dimer may be such a state. This would be consistent with the vibrational distribution seen in desorbed NO. Since redistribution of energy from the weaker modes into the NO stretch is unlikely, the NO vibration is probably excited during an electronic transition. Franck–Condon factors for transition from the ground vibrational state of the A state to the X state are within experimental error of the observed $v=2{:}v=3$ and $v=0{:}v=1$ population ratios.[44] We cannot excite A state monomer, but the transition from NO^+ to NO(X) will have Franck–Condon factors similar to $A \rightarrow X$.

Radiative transition or Förster transfer to a dissociative repulsive region of a lower electronic state, Fig. 14(c), is more likely in the solid than in gas phase dimer dissociation. The weak intermolecular potentials support low frequency local modes and phonons. This "bath" may broaden transitions, increase curve crossing and radiative decay rates, and allow near-resonant energy transfer.

The TOF spectra do not appear to change shape when photon energy is varied from 4.5 to 5.5 eV. This could indicate fast vibrational relaxation in the upper state. Changes in quantum yield and energy distributions with excitation wavelength would be eliminated if relaxation in the vibrational manifold of the excited electronic state is complete before conversion to the dissociative state. In liquids, fluorescence and phosphorescence following electronic excitation are typically independent of excitation wavelength because rapid vibrational relaxation to neighboring molecules ensures that emission is always from the vibrational ground state of electronically excited molecules.[63]

A mechanism for the fast TOF peak consistent with the experimental results, though not necessarily unique, is shown in Fig. 14(d). The dimer is excited to the upper electronic state followed by rapid vibrational relaxation to the bottom of the upper state well. The upper state then internally converts to a promptly dissociative state of the dimer, correlating to ground state monomers with nonstatistical internal excitation.

d. "Hot spot." So far we have considered desorption as dissociation of NO dimers, but any mechanism producing vibrationally excited monomer at the surface of the condensed phase may also lead to desorption. An electronically excited molecule relaxes to high vibrational levels of the ground electronic state. Near-resonant transfer spreads the vibrational excitation to neighboring molecules, creating a small vibrationally excited region. Near the surface, desorption of weakly bound molecules will occur in competition with vibrational relaxation. The NO vibrations at 1900 cm^{-1} would not quickly relax into the lattice, so we might expect desorbing molecules to retain vibrational excitation. We see that the internal energy distribution of desorbed NO is $E_{vib} = 0.4$ eV $> E_{rot} = 0.25$ eV $\geqslant E_{trans} = 0.22$ eV. The photon energy was around 5 eV, and the total energy of each desorbing NO monomer is about 0.8 eV, so up to six molecules could be involved in the hot spot. RRKM theory applied to a related case by Lin *et al.*[13] shows that the translational energy spread in desorbing molecules might be broader than a Maxwellian distribution.

Although the initial electronic excitation has relaxed, this mechanism is still far from thermal equilibrium. Desorption is a single photon process, and the energy distribution of the desorbing molecules cannot be described by a single temperature for all modes.

e. Lattice relaxation. Electronic excitation of NO in the condensed state is accompanied by a change in the effective volume of the excited species. This can induce strain in the surrounding lattice. In the case of NO dimer, the electronically excited state may assume a different equilibrium geometry than in the gas phase. This may modify the dissociation

dynamics, and hence energy disposal in the products. Finally, forces resulting from the dynamic response of the lattice during excited state relaxation may participate in the desorption process.

2. Surface and condensed phase energy transfer

Measurements of desorption yield as a function of varying film thickness and distance to the substrate can be used to probe energy flow within the NO film and to the underlying metal.

For coverages less than 5 ML, we saw a change in the shape of the fast TOF peak, skewing the distribution to lower energies. This might indicate some quenching mechanism close to the metal. However, island formation or other structural changes are also likely to affect the desorption process at low coverage.

For typical film thicknesses we did not observe direct energy transfer to the substrate. We studied the dependence of yield on distance from the NO surface to the metal substrate by using rare gas spacers between the NO and Ag. This is shown in Fig. 10(b). Lack of a significant distance dependence, at least for NO layers thicker than 10 ML, shows that perturbation of yield by the substrate is negligible.

Attenuation of NO signal by rare gas overlayers, Fig. 10(a), implies that fast peak desorption did not come from the bulk NO, but only from the top few layers of the film. The NO yield was reduced by $>90\%$ by 3–5 overlayers of Ar or Kr. (Calculations show that the rare gases should not affect light absorption in the NO.) Some of the rare gas overlayer atoms desorbed during excitation of the underlying NO, probably by a simple kinematic effect of collisions from underlying NO. Ar and NO are not too different in mass, and the TOFs had similar energies. This might also account for the desorption of small amounts of NO dimer.

Since fast peak NO molecules desorb only from the surface of the film, the yield might be expected to saturate for film thicknesses greater than a few layers. But Figs. 9(b) and 9(c) show an increase in desorption with NO thickness to at least 50 ML and possibly several hundred layers before beginning to saturate. If the efficiency of the desorption process was reduced near the underlying metal, we might still expect desorption yield to increase with film thickness, but we have seen that at these coverages desorption was not influenced by distance to the substrate.

The laser penetration depth for 1°–2° glancing incidence is on the order of 100 Å, comparable to the film thickness. Total energy absorbed should increase with film thickness, then saturate for films thicker than the penetration depth. But most of this energy is absorbed in the bulk, and the rare gas overlayer experiments show that NO desorption occurs only from the top few layers of the film, so we have to find a mechanism which increases yield from the surface as film thickness increases. The efficiency of desorption might be greater in thick films, or energy flow from bulk to surface might increase the desorption yield.

The increase in yield with layer thickness might reflect changes in surface morphology. Higher doses could produce rougher surfaces with greater surface area, and therefore greater desorption. In this case thermal annealing would be expected to reduce yield, but angle integrated REMPI measurements show approximately constant yield at annealing temperatures and mass spectrometer measurements at normal show an increase in signal with substrate temperature. Likewise, collision induced changes in the angular distribution cannot contribute significantly to the mass spectrometer signal as a function of layer thickness because angle integrated REMPI measurements show a similar layer thickness dependence.

A temperature dependence of the fast peak desorption efficiency could increase yield with layer thickness since thicker layers might be expected to produce higher surface temperatures from laser heating. This effect would saturate when the film thickness was much greater than the thermal diffusion length during the laser pulse, and the surface temperature reached a maximum. However, a higher than linear laser power dependence would be expected, contrary to observation.

A strong possibility is exciton migration or other nonthermal energy transfer from bulk to surface, followed by desorption. This would increase yield from thick films, even though molecules desorbed only from the top few layers. A photon is absorbed within the film; then the excitation moves by resonant or phonon assisted near resonant electronic or vibrational energy transfer, or perhaps radiation, and decays at the surface, causing desorption. It is known that excitons can diffuse to interfaces where they are trapped and subsequently decay, but this has not been considered as part of a desorption mechanism.[64] We believe that the increase in yield with film thickness, combined with evidence that desorption is only from the top few layers and that yield is independent of distance to the substrate, implies intermolecular energy transfer in electronically excited NO films.

3. Energy balance

In gas phase photodissociation, energy conservation requires that all of the photon energy must appear in the products. On a substrate or in a condensed phase, the molecule is no longer an isolated system, and can exchange energy with the surroundings, so the energy in the desorbed products need not equal the excitation energy. But if we know the energy absorbed and can measure the total product energy then the remainder must be deposited in the film or lost to the substrate.

The linear dependence of fast peak yield on laser pulse energy indicates a single photon desorption mechanism. Ideally, we would be able to account for all of the energy deposited by an incident photon:

$$E_{h\nu} - E_{\text{rad}} = E_{\text{film}} + E_{\text{sub}} + \phi[E_{\text{el}} + E_{\text{vib}} + E_{\text{rot}} + E_{\text{trans}}], \quad (3)$$

where ϕ is the desorption yield, defined as the number of molecules desorbed for each photon absorbed in the surface layer, $E_{h\nu}$ is the photon energy, and E_{rad} is any energy reradiated, E_{film} remains in the thin film of NO, and E_{sub} is transferred to the substrate. The remaining energy is partitioned

among the modes of the desorbing molecules. E_{el} is the average electronic energy, E_{vib} the vibrational energy, E_{rot} the rotational energy, and E_{trans} the translational energy of the desorbed molecules.

We can only roughly estimate the desorption quantum yield. The absolute yield of desorbed molecules is given in Fig. 8 for 223, 247, and 274 nm excitation. If 10% of the incident light is absorbed the yield would be 2×10^{-2} molecules/photon. The desorption probability will vary with the depth at which the photon is adsorbed, but this relationship remains unresolved. We expect that photons absorbed in the first NO layer are very efficient in desorbing NO monomer.

There is about 0.8 eV in each NO desorbed in the fast peak, so a maximum of six molecules could desorb from a single photon. For a desorption mechanism based on dimer dissociation, we must account for 2–3 eV of photon energy. If the excited molecules do not radiate, this energy must have been lost into the surroundings. This is E_{film} which will contribute to bulk heating and the thermal desorption. The internal energy distribution of desorbed NO is $E_{h\nu} = 5.0$ eV $\gg E_{vib} = 0.4$ eV $> E_{rot} = 0.25$ eV $\geqslant E_{trans} = 0.22$ eV. Equipartitioning of the photon energy among the 12 modes of a surface bound dimer would give 0.4 eV of energy in each mode. Coupling between "floppy" vibrations of the dimer and lattice phonons would be strong, but the NO stretch at 1900 cm^{-1} would not quickly relax into the lattice, and shows up in the desorbed products.

Experimental uncertainty in the laser spot size, incident angle, and number of photons absorbed in the surface of the NO layer is large enough to prevent a quantitative determination of overall energy balance. A complete picture of energy balance in the film will also require resolution of the photon energy deposition profile, the role of energy migration within the film, more precise quantum yield measurements, and REMPI spectra of higher vibrational states.

We have only a glimpse into the photochemistry of condensed NO. The incident UV photon excites an electronic state of an NO dimer in the solid. Then a number of things are likely to happen: exciton migration and vibrational relaxation on the excited surface, followed by internal conversion, or perhaps radiative decay, to a vibrationally hot ground state. There may be partial vibrational relaxation on the ground state surface, and low frequency dimer modes couple to phonons. At some point, fragments of dimers near the surface desorb as vibrationally excited electronic ground state monomers. Forces resulting from the dynamic response of the lattice during excited state relaxation may participate in the desorption process. Rotations can be excited as fragments separate, by anisotropic interaction with the surface during desorption, or, for some trajectories, by collisions with the surface. For molecules that cannot reach the surface, the energy of the photon is finally thermalized into bulk heating and thermal desorption.

V. CONCLUSIONS

Condensed nitric oxide absorbs ultraviolet light around 250 nm. We find that UV laser radiation desorbs NO molecules from the surface of a thin film in vacuum and, at higher power, ablates the film. Desorbed NO molecules were studied by mass spectrometer time-of-flight and $(1+1)$ resonance enhanced multiphoton ionization spectroscopy. The broad absorption spectrum of the solid allowed us to both desorb and resonantly, i.e., selectively, detect species using only one tunable laser (a procedure which may be useful in trace chemical analysis at interfaces). We obtained velocity, rotational and vibrational distributions which help elucidate the desorption process. Bimodal TOF distributions provide compelling evidence for two distinct desorption mechanisms. The two mechanisms are distinguished primarily by the energy distributions of desorbing molecules and by the dependence of desorption yield on laser fluence, but also show different responses to film thickness and substrate temperature. By varying the film thickness and laser pulse energy, we could choose experimental regimes in which either mechanism dominates or both are present simultaneously, allowing direct comparison of the two mechanisms. We refer to the two TOF peaks and their associated mechanisms as the fast and slow peaks.

The slow TOF peak dominates when desorption yield per laser pulse is high—for thick films and high laser fluence. The peak can be fit with a Maxwellian velocity distribution at about 200 K, with a near cosine angular distribution. Yield increases exponentially with laser power. At the highest yields, gas phase collisions perturb the slow peak velocity distribution. The slow peak is due to thermal desorption from bulk heating of the film. This heating should depend only on the macroscopic thermal and optical properties of the film, and on the laser spot profile, and not on the initial molecular excitation.

When desorption fluxes are low, only the fast TOF peak is seen. The fast peak is broader than a Maxwellian distribution, with a mean translational energy of 0.22 eV. Desorption flux is peaked toward surface normal. Yield increases linearly with laser fluence, while the fast peak TOF distribution does not seem to vary with laser fluence or wavelength. REMPI spectra show a $v=3{:}v=2$ vibrational population ratio of 0.85, and a rotational distribution for $v=2$ molecules that can be roughly fit with a temperature of 2500 K. The fast peak is due to single photon, nonthermal photochemical desorption. The energy distributions of fast peak molecules are not thermal, nor like those expected from photofragmentation by direct excitation to a repulsive potential energy surface. Instead, we believe the mechanism is complex, with some form of relaxation from the initially excited electronic manifold to vibrationally excited ground state monomer. Desorption may be a result of dissociation of the dimer or vibrational relaxation of the monomer. Comparison of photodesorption from films to photodissociation in the gas phase should be particularly illuminating. Unfortunately, experiments on photofragmentation of NO dimers and clusters at photon energies below the monomer A state threshold are as yet unavailable.

Along with the intramolecular redistribution, there is energy transfer between molecules prior to desorption. Here, desorbed species serve as a probe of energy flow in the condensed phase, as desorption competes with bulk or surface relaxation processes which occur on similar time scales. For

example, we saw that desorption occurred only from the top few layers, but yield increased with film thickness up to several hundred layers, and was independent of distance to the substrate. These results suggest exciton migration or other nonthermal energy transfer from the interior to the surface of the film.

Comparable molecular detail on the effects of laser radiation on complex technological materials, such as polymer photoresists, can be difficult to obtain. We believe that the relatively simple system examined in this paper models important practical aspects of UV photoablation. We have seen that the relative extent of thermal and photochemical effects depends on the amount of laser energy absorbed and on the thermal properties of the system, which in turn reflect the interplay of laser wavelength and power with the optical and thermodynamic characteristics of the film and substrate. All of these factors may have to be taken into account to control the morphology of ablated surfaces of polymers or biological tissues.

ACKNOWLEDGMENTS

We thank Kevin Gibson for invaluable assistance in all aspects of the experiment, Yaw-Wen Yang and Joe Zwanziger for helping test and repair the apparatus. Don Levy and Stuart Rice loaned equipment. Pat Radloff and Edwin Carrasquillo provided a diatomic spectra program. Glenn Tisdale investigated light absorption in thin films. This work was supported in part by The Office of Naval Research, and by the National Science Foundation–Materials Research Laboratory Program at the University of Chicago (NSF-DMR-8519460). W. N. received fellowship support from Dow Chemical U.S.A. and D. P. thanks the Xerox Corp. for support.

APPENDIX: TOF ANALYSIS

It is convenient to describe the amplitude of TOF spectra in terms of molecular flux and characterize their shape by reference to the Maxwell–Boltzmann distribution function. This section describes how the raw data—mass spectrometer counts as a function of time—are fitted to a Maxwellian distribution or related functions, and are converted to absolute molecular flux.

Molecules striking a surface which is in equilibrium with vapor have a Maxwell–Boltzmann velocity distribution and a cosine angular flux distribution. By microscopic reversibility, the total distribution of molecules leaving the surface, which includes both those desorbed and scattered, must be identical to the incident distribution (with normal velocity terms reversed). The rate per unit surface area at which molecules strike the surface is[65]:

$$\frac{d^2N}{dAdt} = \frac{\rho}{4\pi}\int_0^{2\pi} d\phi \int_0^{\pi/2} \cos\theta \sin\theta \, d\theta \times \int_0^{\infty} 4\pi \left(\frac{m^2}{2\pi kT}\right)^{3/2} \exp\left(-\frac{mc^2}{2kT}\right) c^3 \, dc, \tag{A1}$$

where m is the mass of the molecule, k is Boltzmann's constant, T is the temperature in Kelvin, ρ is the molecular density, and c is the molecular velocity.

The normalized flux TOF distribution is

$$\frac{1}{N}\frac{d^3F(\theta,\phi,t)}{d\theta\, d\phi\, dt} = \frac{1}{2}\cos\theta \sin\theta \times \left(\frac{m}{kT}\right)^2 \frac{x^4}{t^5} \exp\left(-\frac{mx^2}{2kTt^2}\right). \tag{A2}$$

We assume that the desorption pulse length is small compared to the flight time to the detector and the entire active surface is contained in the viewing area of the detector at normal incidence. For a number density detector, such as a mass spectrometer, with an aperture of solid angle $d\Omega$ at distance x from the surface:

$$C = \int S(t)dt = N\int_\Omega \frac{\cos\theta}{2\pi} d\Omega \int_0^{\infty} \eta \Delta x \frac{t}{x} \times \left(\frac{m}{kT}\right)^2 \frac{x^4}{t^5} \exp\left(-\frac{mx^2}{2kTt^2}\right) dt, \tag{A3}$$

where C is the total number of counts, $S(t)$ is the count rate as a function of time, η is the detection efficiency in counts/molecule/s and $\Delta x_{\frac{t}{x}}$ is the travel time within the detection region (mass spectrometer ionizer) Δx cm long.

For a 1.0° diameter detector aperture ($7.6\times10^{-5}\pi$ sr) at crystal normal, Eq. (A3) becomes

$$C = N\eta\Delta x \left(\frac{m\pi}{8kT}\right)^{1/2} 7.6\times10^{-5}. \tag{A4}$$

The mass spectrometer can be calibrated by thermal desorption of an NO layer of known thickness. If the sticking coefficient is unity for molecules incident on a film in equilibrium at the desorption temperature, then the flux distribution of desorbing molecules will be given by Eq. (A3) and the number of counts by Eq. (A4). The only unknown is the ionization efficiency $\eta\Delta x$. Desorption of one layer from a 2.0 mm^2 spot, or 1.7×10^{13} molecules at 52 K produces 12 000 counts in $7.6\times10^{-5}\pi$ sr at the normal angle. The fraction of desorbed molecules passing through the detector at normal for a cos θ angular distribution is 7.6×10^{-5}. The detection efficiency for NO is 9.2×10^{-6}. Equation (A4) yields 0.18 counts cm/s molecule for $\eta\Delta x$ and 1.2 counts/s molecule for η for an ionizer length of 1.5 mm.

We fit the laser desorption TOF data (cnts bkgd)s^{-1} shot^{-1} to a sum of three shifted Maxwellian velocity distributions with different angular dependencies:

$$S(\theta,\phi,t) = \sum_{i=1}^{3} C_i \cos^{n_i}\theta \frac{x^3}{t^4} \times \exp\left\{-\frac{m[(x/t)-v_i]^2}{2kT_i}\right\}. \tag{A5}$$

In most cases the stream velocities v_i were fixed at zero and T_1 and T_2 were held constant. The C_i were determined at crystal normal, and then fixed when the $\cos^{n_i}\theta$ terms were fit to TOFs off normal. The parameters should be related to the number of molecules by

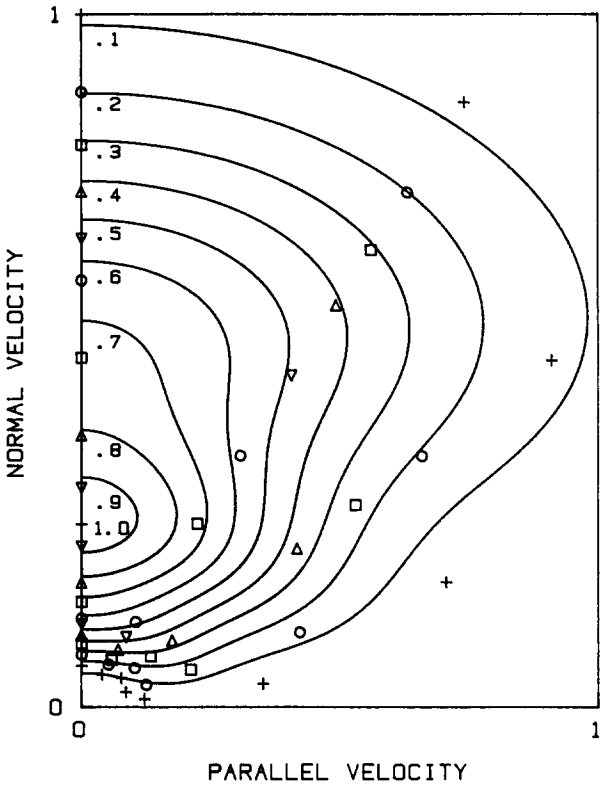

FIG. 15. Flux contours vs velocity. Desorption conditions as in Fig. 3. The fast peak accounted for 75% of total yield with a 1.8:1 ratio of high and low energy terms and the slow peak contained 25% of total yield. Sections along each angle correspond to Fig. 3(a). The fit is from Eq. (A5): the fast peak low energy and high energy terms were fit with 525 K $\cos^2\theta$ and 1925 K $\cos^4\theta$ distributions, while the slow peak was 180 K $\cos\theta$.

$$C_i = 7.6\times10^{-5}\,\frac{n_i+1}{2}\sqrt{\frac{m\pi}{8kT_i}}\,N_i\eta\Delta x.$$

The data and fits were then transformed to flux weighted time, velocity, and energy distributions. Figure 15 shows a contour plot of desorption flux in velocity space with fit.

The average translational energy of the fast peak calculated from the flux weighted angular and TOF distributions is

$$\langle E_T\rangle = \frac{1}{N}\sum_{i=1}^{2}\int_\Omega\int_0^\infty \frac{mx^3}{2t^3}\,S_i(\theta,\phi,t)\,d\Omega\,dt, \qquad \text{(A6)}$$

where index i labels the high and low energy terms of the fast peak fit.

[1]R. Srinivasan, Science **234**, 559 (1986), and references therein.
[2]T. J. Chuang, Surf. Sci. Rep. **3**, 1 (1983), and references therein.
[3]J. P. Cowin, D. J. Auerbach, C. Becker, and L. Wharton, Surf. Sci. **78**, 545 (1978).
[4]G. Wedler and H. Ruhmann, Surf. Sci. **121**, 464 (1982).
[5]D. Burgess, Jr., R. Viswanathan, I. Hussla, P. C. Stair, and E. Weitz, J. Chem. Phys. **79**, 5200 (1983).
[6]D. Burgess, Jr., D. A. Mantell, R. R. Cavanaugh, and D. S. King, J. Chem. Phys. **85**, 3123 (1986).
[7]M. P. Casassa, E. J. Heilweil, J. C. Stephenson, and R. R. Cavanaugh, J. Chem. Phys. **84**, 2361 (1986).
[8]R. Rossetti and L. E. Brus, J. Chem. Phys. **73**, 572 (1980).
[9]A. P. Alivistos, D. H. Waldeck, and C. B. Harris, J. Chem. Phys. **82**, 541 (1985).
[10]J. Heidberg, H. Stein, E. Riehl, Z. Szilágyi, and H. Weiss, Surf. Sci. **158**, 553 (1985).
[11]T. J. Chuang, H. Seki, and I. Hussla, Surf. Sci. **158**, 525 (1985), and references therein; I. Hussla, H. Seki, T. J. Chuang, Z. W. Gortel, H. J. Kreuzer, and P. Piercy, Phys. Rev. B **32**, 3489 (1985).
[12]E. Hood, C. Jedrzejek, K. F. Freed, and H. Metiu, J. Chem. Phys. **81**, 3277 (1984).
[13]S. H. Lin, A. Boeglin, B. Fain, and C-Y. Yeh, Surf. Sci. **180**, 289 (1987), and references therein.
[14]Faraday Discuss Chem. Soc. **58** (1974).
[15]F. A. Houle, J. Chem. Phys. **79**, 4237 (1983).
[16]T. J. Chuang, J. Vac. Sci. Technol. **21**, 798 (1982).
[17]R. M. Osgood, Jr., Annu. Rev. Phys. Chem. **34**, 77 (1983).
[18]D. J. Ehrlich and J. Y. Tsao, J. Vac. Sci. Technol. B **1**, 969 (1983).
[19]G. M. Goncher, C. A. Parsons, and C. B. Harris, J. Phys. Chem. **88**, 4200 (1984).
[20]J. H. Brannon, J. R. Lankard, A. I. Baise, F. Burns, and J. Kauffman, J. Appl. Phys. **58**, 2036 (1985).
[21]P. E. Dyer and J. Sidhu, J. Appl. Phys. **57**, 1420 (1985).
[22]R. Srinivasan and V. Mayne-Banton, Appl. Phys. Lett. **41**, 576 (1982).
[23]G. Koren and J. T. C. Yeh, J. Appl. Phys. **56**, 2120 (1984).
[24]W. Sesselmann and T. J. Chuang, Surf. Sci. **162**, 1007 (1985).
[25]W. Sesselmann and T. J. Chuang, J. Vac. Sci. Technol. B **3**, 1507 (1985).
[26]N. Nishi, H. Shinohara, and T. Okuyama, J. Chem. Phys. **80**, 3898 (1985).
[27]E. B. D. Bourdon, J. P. Cowin, I. Harrison, J. C. Polanyi, J. Segner, C. D. Stanners, and P. A. Young, J. Phys. Chem. **88**, 6100 (1984).
[28]F. L. Tabares, E. P. Marsh, G. A. Bach, and J. P. Cowin, J. Chem. Phys. **86**, 738 (1987).
[29]E. P. Marsh, F. L. Tabares, M. R. Schneider, and J. P. Cowin, J. Vac. Sci. Technol. (to be published).
[30]N. Nishi, M. Kawasaki, and T. Okuyama, *Annual Review of the Institute for Molecular Science* (Okazaki, Japan, 1985), p. 64.
[31]P. Avouris and B. N. J. Persson, J. Phys. Chem. **88**, 837 (1984).
[32]J. W. Gadzuk, J. Chem. Phys. **79**, 6341 (1983).
[33]C. T. Rettner, F. Fabre, J. Kimman, and D. J. Auerbach, Phys. Rev. Lett. **55**, 1904 (1985).
[34]C. A. Becker, Ph.D. thesis, The University of Chicago, 1980.
[35]C.-F. Yu, K. B. Whaley, C. S. Hogg, and S. J. Sibener, J. Chem. Phys. **83**, 4217 (1985).
[38]K. D. Gibson and S. J. Sibener, Phys. Rev. Lett. **55**, 1514 (1985).
[37]R. J. Behm and R. C. Brundle, J. Vac. Sci. Technol. A **2**, 1040 (1984).
[38]J. Granier-Mayence and J. Romand, C. R. **258**, 1148 (1953).
[39]W. N. Lipscomb, F. E. Wang, W. R. May, and E. L. Lippert, Jr., Acta. Crystallogr. **14**, 1100 (1961).
[40]W. N. Hansen, J. Opt. Soc. Am. **58**, 380 (1968).
[41]J. A. Stratten, *Electromagnetic Theory* (McGraw–Hill, New York, 1941).
[42]D. C. Jacobs and R. N. Zare, J. Chem. Phys. **80**, 5457 (1986).
[43]D. C. Jacobs, R. J. Madix, and R. N. Zare, J. Chem. Phys. **80**, 5469 (1986).
[44]D. C. Jain and R. C. Sahni, Trans. Faraday Soc. **64**, 3169 (1968).
[45]J. M. Green, W. T. Silfrast, and D. R. Wood, J. App. Phys. **48**, 2753 (1977).
[46]R. E. Walkup, J. M. Jasinski, and R. W. Dreyfus (private communication).
[47]R. W. Dreyfus, R. Kelly, and R. E. Walkup (private communication).
[48]A. S. Sudbo and M. M. T. Loy, J. Chem. Phys. **76**, 3646 (1982).
[49]A. S. Sudbo and M. M. T. Loy, Chem. Phys. Lett. **82**, 135 (1981).
[50]J. C. Stephenson, J. Chem. Phys. **59**, 1523 (1973).
[51]M. Buck, B. Schäfer, and P. Hess, Surf. Sci. **161**, 245 (1985).
[52]J. L. Brand and S. M. George, Surf. Sci. **167**, 341 (1986).
[53]J. F. Ready, *Effects of High Power Laser Radiation* (Academic, New York, 1971).
[54]*Moving Boundary Problems*, edited by D. G. Wilson, A. D. Solomon, and P. T. Boggs (Academic, New York, 1978).
[55]*Handbook of Chemistry and Physics*, 52nd ed. (Chemical Rubber, Cleveland, 1971), p. D-174.

[56]U.S. Bureau of Mines Bulletin **601** (1962).
[57]E. Forte and H. Van Den Berg, Chem. Phys. **30**, 325 (1978).
[58]J. Billingsley and A. B. Callear, Trans. Faraday Soc. **67**, 589 (1970).
[59]Y. Haas and M. Asscher, in *Photoselective Chemistry*, Vol. 47 of *Advances in Chemical Physics*, edited by J. Jortner, R. D. Levine, and S. A. Rice (Wiley, New York, 1981), Part 2.
[60]E. Carrasquillo, Ph.D. thesis, Department of Chemistry, University of Chicago, 1984.
[61]W. M. Gelbart and R. Bersohn, Annu. Rev. Phys. Chem. **28**, 323 (1977).
[62]G. E. Busch and K. R. Wilson, J. Chem. Phys. **56**, 3626 (1972).
[63]N. J. Turro, V. Ramanmurthy, W. Cherry, and W. Farneth, Chem. Rev. **78**, 125 (1978).
[64]M. Ueta, *Excitonic Processes in Solid* (Springer, New York, 1986), Vol. 60.
[65]F. O. Goodman and H. Y. Wachman, *Dynamics of Gas–Surface Scattering* (Academic, New York, 1976).